JOURNAL OF CHEMICAL INFORMATION AND MODELING

Article

pubs.acs.org/jcim

Intermolecular Sulfur···Oxygen Interactions: Theoretical and Statistical Investigations

Xuejin Zhang,[†] Zhen Gong,[‡] Jian Li,*[,‡] and Tao Lu*[,†]

[†]School of Basic Science, China Pharmaceutical University, No. 24 Tongjiaxiang, Nanjing 210009, P. R. China

[‡]State Key Laboratory of Lead Compound Research, WuXi AppTec, 288 Fute Zhong Road, Waigaoqiao Free Trade Zone, Shanghai 200131, China

Supporting Information

ABSTRACT: Intermolecular S···O interactions are very common and are important in biological systems, but until recently, the presence of these contacts in protein−ligand systems largely depended on serendipitous discovery instead of rational design. Here we provide insight into the phenomenon of intermolecular S···O contacts by focusing on three sulfur-containing aromatic rings. Quantum mechanics is employed to characterize the strength and directionality of the S···O interactions and to determine their energy dependence on their geometric parameters. Protein Data Bank mining is performed to systematically determine the occurrence and geometry of intermolecular S···O interactions, and several representative examples are discussed. Three typical cases are investigated using a combined quantum mechanics/molecular mechanics approach to demonstrate the potential of these interactions in improving binding affinities and physiochemical properties. Overall, our work elucidates the structures and energy features of intermolecular S···O interactions and addresses their use in molecular design.

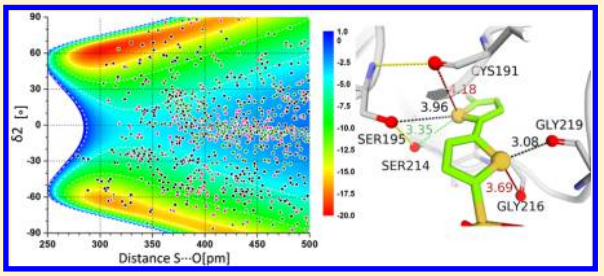

INTRODUCTION

Heteroaromatic rings containing sulfur have been key components in medicinal chemistry for decades. Until recently, they were described as hydrophobic moieties that participate in well-studied interactions such as $\pi-\pi$ stacking, cation$-\pi$, and halogen$-\pi$ interactions.[1−3] Intriguingly, atypical close contacts between sulfur atoms on heteroaromatic scaffolds and oxygen atoms have received increasing attention. In these interactions, the sulfur atom acts as a Lewis acid despite its electronegativity. These interactions are most likely driven by HOMO−LUMO and Coulomb interactions.[4] The highly versatile sulfur atom has a net positive charge due to the donation of its p_z electrons to the aromatic π system.[5] Therefore, it acts like an "electrophile" as it approaches the electronegative oxygen atom, forming a favorable interaction between the n_O HOMO and σ^*_S LUMO in the opposite direction of the S−X bond (where X is an electronegative or polarizable "counteratom").[4,6] Because the electron-deficient outer lobes are directed along the same axis as the half-filled p bonding orbitals, in 2008 Murray et al.[7] attributed this attractive S···O interaction to σ-hole bonding. Moreover, by conducting a computational study of a series of sulfur heterocycles, they distinguished between sulfur atoms that could produce σ holes with a positive electrostatic potential and sulfur atoms substituted with electron-withdrawing groups (e.g., −F, −Cl, −CN, or π electrons).

Over the past 40 years, a considerable amount of experimental data has indicated the existence of sulfur−oxygen interactions. As early as 1977, Rosenfield et al.[8] first noted the versatile features of a sulfur atom. They analyzed both intra- and intermolecular S−O interactions in organic and inorganic crystal structures and suggested that the nucleophilic O atom tends to attack the divalent sulfur atom (Y−S−Z) along the direction of the S−Y or S−Z bond (the σ^*_S direction). Before 1983, approximately 400 crystalline compounds with intramolecular S···O contacts (203−300 pm) that are significantly shorter than the sum of their corresponding van der Waals radii (335 pm) were catalogued according to Ángyán and Kucsman.[6] In 1985, a search of the Cambridge Crystallographic Database (CCD) by Kucsman and Kapovits[9] revealed 750 structures containing close intramolecular sulfur−oxygen contacts between 200 and 325 pm. A 1991 survey of the CCD by Markham and Bock[10] yielded 144 additional structures containing intramolecular 1,4-type S···O contacts (i.e., contacts between sulfur and oxygen atoms connected through two atoms) of less than 330 pm. Iwaoka et al.[11] conducted a comprehensive search for intra- and intermolecular S···O interactions in 2002 and found that totals of 1200 and 626 fragments have close intramolecular S···O interactions (S···O distances of ≤352 pm) in the Cambridge Structural Database (CSD) and Protein Data Bank (PDB), respectively.

Unfortunately, most of these studies focused on the effects of close S···O contacts on the molecular conformation.[4,5,9,12] For example, Burling and Goldstein[5] demonstrated the electrostatic nature of the 1,4-type intramolecular S···O interactions by studying the thiazole nucleoside and its effect on maintaining

Received: April 1, 2015
Published: September 22, 2015

DOI: 10.1021/acs.jcim.5b00177
J. Chem. Inf. Model. 2015, 55, 2138−2153

particular binding modes. Kucsman and Kapovits[9] explored the directional preferences of intramolecular 1,3-, 1,4-, and 1,5-type S···O interactions and identified many factors that control the S···O distance.

However, S···O interactions not only control molecular conformations but also affect ligand−receptor binding modes, which in turn might affect protein structures, stabilize folded protein structures,[11] regulate enzymatic function,[13] influence the biological activities of some sulfur-containing organic compounds, etc. Thus, a global analysis of intermolecular S···O interactions is needed.

In this work, quantum mechanics (QM) is used to characterize the strengths of the interactions between *N*-methylacetamide and the sulfur atom in the three most frequently used sulfur-containing aromatic scaffolds: thiophene, thiazole, and thiadiazole. On the basis of our model calculations, simple rules are deduced to characterize the intermolecular S···O interactions. Additionally, the impact of the geometric parameters on the overall complex formation energies is elucidated. The occurrence of intermolecular S···O interactions in biological systems is determined by a comprehensive analysis of the PDB, and typical examples of desirable intermolecular S···O interactions are described. Finally, by means of a combined quantum mechanics/molecular mechanics (QM/MM) approach, the potential application of these interactions in drug design is explored.

1. DATA MINING FOR THE THREE SULFUR-CONTAINING AROMATIC RINGS

Taylor et al.[14] analyzed the ring structures in the drugs listed in the FDA Orange Book from 1983 to 2012. According to their analysis, thiazole and thiophene rings are among the top 20 most frequently used ring systems (the thiazole scaffold has been used 25 times and is ranked 12th, and thiophene has been used 16 times and is ranked 19th), and the relatively novel thiadiazole scaffold, which has been used only four times, was among the top 100 rings.

We performed data mining of the worldwide Cortellis database[15] and found that 51 launched small-molecule drugs (with diverse structures) include a thiophene ring and 53 launched drugs have a thiazole moiety. Thiadiazole, however, appears in only one launched antibacterial drug. Remarkably, only five of the 51 thiophene-containing drugs and four of the 53 thiazole-containing drugs were withdrawn from the market. Moreover, two promising thiadiazole-containing drugs are now in clinical trials. Data mining of the PDB[16] revealed that 612 different ligands contain a thiophene moiety, 532 include a thiazole ring, and 37 involve a thiadiazole moiety. The data mining results are summarized in Table 1.

Table 1. Data Mining for the Three Sulfur-Containing Aromatic Rings in Launched Drugs or in Ligands in the PDB

		Cortellis[b]		
scaffold	FDA Orange Book[a]	launched	withdrawn	PDB[c]
thiophene	16	51	5	612
thiazole	25	53	4	532
thiadiazole	4	1	0	37

[a]Data obtained by Taylor et al.[14] from the FDA Orange Book. [b]Numbers of drugs on the market catalogued from the Cortellis Web site.[15] [c]Numbers of ligands with unique structures compiled from the PDB.

These three sulfur-containing aromatic scaffolds have extensive biological activity profiles. For example, the very versatile architectural constituent thiophene is found in drugs used to treat various conditions, including those of the cardiovascular, dermatological, endocrine, respiratory, nervous, genitourinary, and sex hormone systems and of sensory, blood, and blood-forming organs.[17] Thiadiazole is used in various applications as pharmaceuticals, oxidation inhibitors, cyanine dyes, and metal-complexing agents.[18]

On the basis of the above data mining results, thiophene, thiazole, and thiadiazole are undoubtedly fundamental building blocks of small-molecule drugs on the market. They are also key components that contribute to the drugs' physicochemical properties, such as the electronic distribution, scaffold rigidity, lipophilicity, and polarity, which determine their molecular reactivities and druggabilities. Despite potential limitations, these advantages make sulfur-containing heterocycles very useful for improving molecular recognition and pharmacokinetics properties in drug design.

2. METHODS

2.1. QM Calculations. All of the dispersion-corrected density functional theory (DFT-D) calculations in this work were performed using Jaguar 8.5 as implemented in Schrödinger 2014-2.[19] The natural bond orbital (NBO) analyses were performed using the NBO 6.0 program[20] in the Maestro interface. The M06-2X functional developed by Zhao and Truhlar,[21] which is parametrized for non-covalent interactions (NCIs), kinetics, etc., was employed in the calculations. This functional was augmented with an empirical dispersion correction, indicated by appending "-D3" to the name as proposed by Grimme.[22] The revised DFT-D3 method is a general tool for including the dispersion energy in electronic structure calculations of large systems.[23] The 6-31++G** basis set[24−29] was used. The "**" indicates that polarization functions were used to model all of the atoms except transition-metal atoms, whereas the "++" indicates that diffuse functions were placed on all of the atoms. The basis set superposition errors (BSSEs) of the interaction energies were corrected using the counterpoise method proposed by Boys and Bernardi.[30] The M06-2X-D3/6-31++G** method was used for the structural optimizations, construction of electrostatic potential surfaces, NCI analyses, NBO analyses, and potential energy surface scans. The M06-2X-D3/6-311G-3df-3pd[31−34] method was used for the molecular orbital analysis. Energy decomposition analysis was performed using the GAMESS program[35−37] at the M06-2X/6-31++G** level.

2.2. QM/MM Calculations. All of the QM/MM calculations in this work were performed using QSite 6.2.[38] Before the energy minimization was performed, the force field used to model the ligand and protein and their charges were assigned using the Prime 3.6 program.[39] The energy of the MM layer, which was modeled with the OPLS-2005 force field,[40,41] was minimized using a truncated Newton method, while the energy of the QM layer was minimized at the M06-2X/6-31G* level, except for the zinc ion in the protein pocket, which was represented by the LAV3P[42,43] basis set. The OPLS-2005 force field is known to be accurate, and the M06-2X method was used because the revised M06-2X-D3 method is not available in QSite. The smaller 6-31G* basis set was used for the QM layer because of the increased computational cost. Residues containing an oxygen atom that is within 500 pm of a ligand sulfur atom (or oxygen atom) and the ligand were included in

DOI: 10.1021/acs.jcim.5b00177
J. Chem. Inf. Model. 2015, 55, 2138−2153

the QM region. The minimized conformations of the complexes were employed for the binding energy calculations. Single-point energy calculations on the ligand and on the protein in the QM layer were performed separately at the same level of theory as the structure optimization.

The interaction energy between the ligand and the protein, ΔE, was calculated using eq 1:

$$\Delta E = \Delta E_{\text{complex}} - (\Delta E_{\text{ligand}} + \Delta E_{\text{protein}}) \quad (1)$$

where $\Delta E_{\text{complex}}$, ΔE_{ligand}, and $\Delta E_{\text{protein}}$ are the energies of the complex, ligand, and protein, respectively.

2.3. Potential Energy Surface Scans. *2.3.1. Distance Scans.* Starting from the minimum-energy structures obtained at the M06-2X-D3/6-31++G** level, the distance scans were performed in the S···O direction. For the context model, which has only a C_R−H···O═C contact between *N*-methylacetamide and the thiophene C−H in the S−C_2 bond direction, the distance scan was performed in the C−H···O direction. The $d_{S/H\cdots O}$ distances were increased in steps of 2 pm from 240 to 340 pm, steps of 5 pm from 340 to 420 pm, and steps of 10 pm from 200 to 240 pm and from 420 to 500 pm.

2.3.2. σ-Hole Angle Scans. The scan of the angle for approach of the amide carbonyl to the aromatic ring was started from the conformation in which the sulfur position was fixed at an optimal distance with α(C1−O1···S) = 0° and α(O1···S1···Q2) = 90° (Figure 1a). These constraints were used to avoid redundant interactions between the aromatic ring and the methyl moiety of the backbone system. The σ-hole angle α(O1···S1···Q1) was increased in steps of 5° from 0° to 180°, except in the ranges of 50° to 70° and 140° to 160°, where the angle was increased in steps of 2°. A new dummy atom Q3 was introduced to better illustrate the symmetry of thiophene and thiadiazole and the asymmetry of thiazole (Figure 1b). Thus, the angle used to construct the final curve was α(O1···S1···Q3) = 90° − α(O1···S1···Q1).

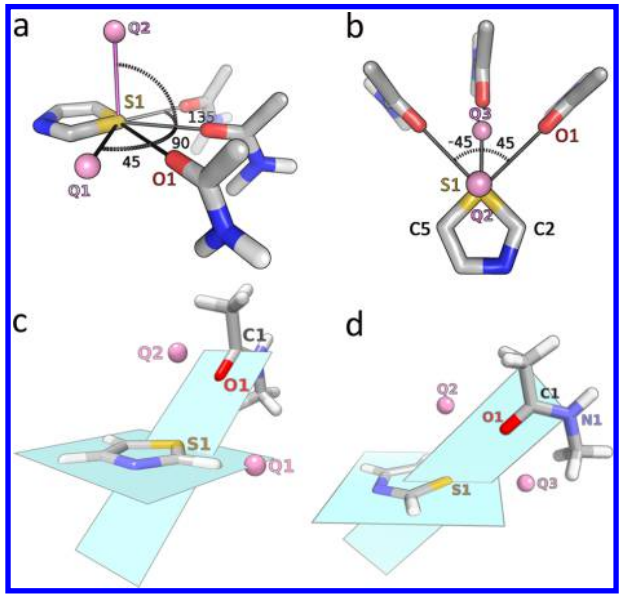

Figure 1. (a) Illustration of the σ-hole angle scan setup. The model ligand system is rotated around the axis perpendicular to the thiazole plane that passes through the sulfur atom. (b) Representative model. In the thiazole system, when the carbonyl oxygen is near C2 (or along the C5−S bond direction), α(O1···S1···Q3) is positive; when the carbonyl oxygen is near C5 (or along the C2−S bond direction), the angle is negative. (c) Illustration of the angle δ1 (out-of-plane rotation). The out-of-plane angle δ1 the angle between the S1···O1 bond and the plane containing the thiazole ring. (d) Illustration of the angle δ2 (in-plane rotation). The in-plane angle δ2 is the angle of rotation of the S1···O1 bond around the Q2···S1 axis. If the rotation of the S1···O1 bond is clockwise, the value of δ2 is positive; if the rotation of the S1···O1 bond is counterclockwise, the value of δ2 is negative.

2.3.3. Combined Distance and Angle Scans. The models used in the σ-hole angle scan were employed in the combined distance and angle scans. The $d_{S\cdots O}$ distance was increased in steps of 10 pm from 250 to 500 pm. At each distance, the σ-hole angle α(O1···S1···Q1) was increased in steps of 5° from 0 to 90° for the thiophene system and from 0° to 180° for the thiazole system. Because of the symmetry of the thiophene system observed in the σ-hole angle scan, the range from 90° to 180° was omitted to reduce the computational cost.

2.3.4. Spherical Scans. Starting from the initial geometries used in the σ-hole angle scan, the out-of-plane angle δ1 was increased in steps of 5° from −90° to 90° (Figure 1c). At each δ1, the in-plane angle δ2 was increased in steps of 5° from −90° to 90° (Figure 1d). When δ1 = 0°, the in-plane angle δ2 is equal to the σ-hole angle α(O1···S1···Q3).

2.4. PDB Mining. On the basis of the model system geometries described in Figure 1, Python scripts were written to extract all contacts between sulfur atoms on ligand aromatic rings and protein oxygen atoms from the recent version of the PDB (December 2014). For all three systems, the range of the out-of-plane angle δ1 from −90° to 0° was mapped onto its range from 0° to 90° because of the symmetry of the ring planes. For the thiophene and thiadiazole systems, the range of the in-plane angle δ2 from −90° to 0° was mapped onto the range from 0° to 90° on the basis of their mirror symmetry. The distance cutoffs were 250 pm ≤ $d_{S\cdots O}$ ≤ 500 pm because no favorable binding energies were observed outside that range. Multiple Lewis bases were found within the searched spherical volume. The spherical orientations were divided into three categories: 90° to 60°, 60° to 30°, and 30° to 0°. Within each range, similar trends in the interaction strength were observed.

2.5. Visualization. For visualization purposes, several Python scripts were written and executed in PyMOL 1.5.0.4.[44] The interaction energies were represented using a color spectrum (red to blue to purple). Several compiled graphic objects (CGOs)[45] with the appropriate coloring were generated as virtual planes. Some of the structures were prepared with Maestro 9.4.[46]

3. NATURE OF THE INTERACTIONS BETWEEN LIGAND SULFUR AND PROTEIN OXYGEN ATOMS

The strengths of sulfur−oxygen interactions can be evaluated theoretically with QM calculations. Here the carbonyl oxygen moiety of the protein was used in the model calculations because ligand sulfur atoms most frequently bind to it. Thiophene, thiazole, and thiadiazole were employed as the ligand models because these sulfur-containing heteroaromatic scaffolds are common cores in medicinal chemistry and are widely exploited in scaffold-hopping data mining methods. Different QM methods and basis sets were tested using the thiazole-C5 model system (Table S1 in the Supporting Information). A comparison of different basis sets revealed that the results obtained with either 6-31++G** or 6-311++G** are very similar to those obtained with aug-cc-pVTZ. Because the aug-cc-pVTZ basis set is computationally expensive (time-consuming) and the 6-311++G** basis set is not

DOI: 10.1021/acs.jcim.5b00177
J. Chem. Inf. Model. 2015, 55, 2138−2153

Table 2. M06-2X-D3/6-31++G** Interaction Energies of Sulfur−Oxygen Contact Model Systems

complex	method	ΔE (kJ/mol)[a]	$d_{S\cdots O}$ (pm)	$\alpha(C_{ar}-S-O)$ (deg)	$\alpha(S-O-C(BB))$ (deg)
thiophene···BB[b]	M06-2X-D3/6-31++G**	−21.8	324	153.1	81.8
thiazole-C5[c]···BB	M06-2X-D3/6-31++G**	−22.6	305	159.4	136.0
thiazole-C2[d]···BB	M06-2X-D3/6-31++G**	−22.9	319	156.2	85.0
thiadiazole···BB	M06-2X-D3/6-31++G**	−26.9	302	156.2	138.3
oxazole···BB	M06-2X-D3/6-31++G**	−11.1	331[e]	178.6	175.9
BB···BB	M06-2X-D3/6-31++G**	−38.0	N/A	N/A	N/A

[a]Interaction energies with BSSEs corrected using the counterpoise method. [b]BB = *N*-methylacetamide (the "backbone" model). [c]Thiazole-C5: the backbone carbonyl oxygen is located along the C5−S bond direction. [d]Thiazole-C2: the backbone carbonyl oxygen is located along the C2−S bond direction. [e]Distance between the oxygen of the oxazole ring and the oxygen of BB.

available in the QSite 6.2 program, the 6-31++G** basis set was chosen for this study. An analysis of the first three rows in Table S1 shows that an additional constraint was required to obtain locally converged results when the LMP2 method was used. The widely employed B3LYP-D3 functional slightly underestimated the strength of the S···O interactions because the calculated S···O distance was larger than the sum of their van der Waals radii (~335 pm). In contrast, the interaction distance in the model system was calculated to be significantly smaller than 335 pm by the M06-2X-D3 method. Thus, the M06-2X-D3/6-31++G** level of theory yielded qualitatively correct geometries.

3.1. Strength of the Interactions between Ligand Sulfur and Protein Oxygen Atoms. A typical hydrogen bond has an energy of 22−30 kJ/mol (e.g., the one in the H_2O dimer has an energy of approximately 24 kJ/mol and the one between H_2O and NH_3 has an energy of approximately 30 kJ/mol.) According to Table 2, the interaction strength of the complex between thiadiazole and *N*-methylacetamide (the backbone (BB) model) is 26.9 kJ/mol, which is similar to that of a moderately strong hydrogen bond. Likewise, the S···O interactions in the thiazole and thiophene complexes (22.6 or 22.9 and 21.8 kJ/mol, respectively) are comparable to that of a typical hydrogen bond. While this result is quite striking, it is likely that interactions other than the S···O contact also contribute to the complex formation energy, as indicated by the optimized geometries of the complexes (Figure 2). In all of the complexes, the carbonyl oxygen does not interact with the sulfur-containing aromatic rings in an ideal "head-on" fashion in which the C_{ar}−S···O angle is close to 180°. Instead, the C_{ar}−S···O angle ranges from 150° to 160°, and the oxygen is located between the hydrogen and sulfur atoms. The unusually high binding strength and nonideal geometries indicate that multiple interactions between the two molecules occur and that both the hydrogen and sulfur atoms probably interact with the carbonyl oxygen.

A non-covalent interaction (NCI) analysis of the optimized thiazole−acetamide complex was performed to elucidate all of the interactions between the two molecules. Three possible interactions between thiazole and *N*-methylacetamide include acetamide hydrogen−thiazole sulfur, acetamide carbonyl oxygen−thiazole hydrogen, and acetamide carbonyl oxygen−thiazole sulfur interactions (Figure S1 in the Supporting Information). On the basis of the interaction strengths, the first interaction is weak compared with the other two interactions. This result supports our earlier hypothesis of the existence of multiple interactions. Thus, the complex conformation is best stabilized by allowing the oxygen to interact with the adjacent sulfur and hydrogen atoms of the aromatic system simultaneously by occupying the space between them.

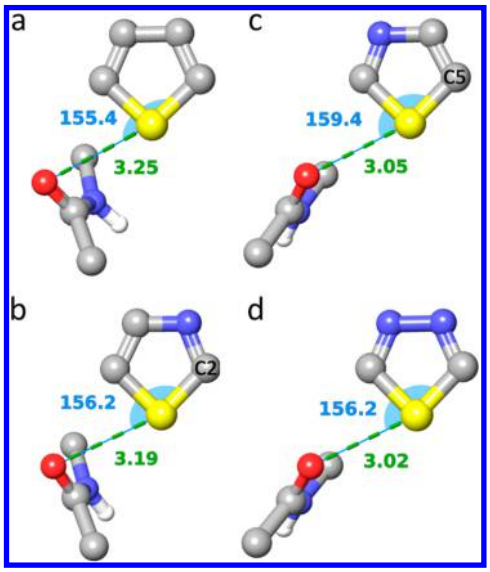

Figure 2. Conformations optimized at the M06-2X-D3/6-31++G** level: (a) thiophene···*N*-methylacetamide; (b) thiazole-C2···*N*-methylacetamide (carbonyl oxygen along the thiazole C2−S bond direction); (c) thiazole-C5···*N*-methylacetamide (carbonyl oxygen along the thiazole C5−S bond direction); (d) thiadiazole···*N*-methylacetamide.

3.2. Tuning of the Strength of the Interactions between Ligand Sulfur and Protein Oxygen Atoms. The electrostatic potential (ESP) maps computed for these sulfur-containing heteroaromatic systems (Figure 3) reveal overlapping positively charged regions, called σ holes, along the S−C bond directions and around the hydrogen atoms. Both the hydrogen and sulfur atoms contribute to the σ hole, and the most positive point on the ESP map is located between these two atoms, which is consistent with the NCI analysis. The σ hole is relatively more positive than the other electron-deficient areas on the aromatic rings, in contrast to sulfur atoms bonded to halogens, which are surrounded by an electron-rich belt.

As the number of electron-withdrawing nitrogen atoms in the ring increases, the σ holes increase in size, and the highest ESP observed for each of the three scaffolds also increases (as indicated by the color transition in Figure 3). The asymmetry of thiazole leads to different potentials on the two sides of the sulfur atom in the ring. The highest ESP along the C2−S bond is higher than that along the C5−S bond. Accordingly, the conformations obtained from the QM optimizations are also distinct. Along the C2−S bond direction, the carbonyl oxygen is closer to the hydrogen atom, as observed in the thiophene complex (Figure 2a,b), but it moves closer to the sulfur atom along the C5−S bond direction, which is similar to the

DOI: 10.1021/acs.jcim.5b00177
J. Chem. Inf. Model. 2015, 55, 2138−2153

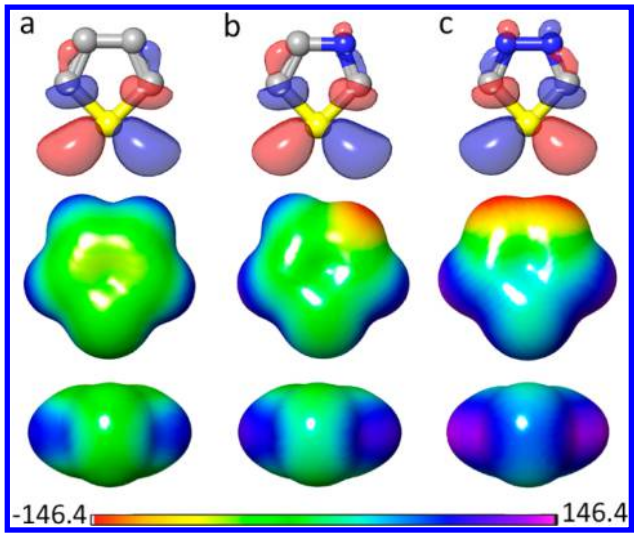

Figure 3. LUMO+1 molecular orbitals and ESP surfaces: (a) thiophene (E = 1.455 eV); (b) thiazole (E = 1.091 eV); (c) thiadiazole (E = 0.6851 eV). The color gradient from red to violet represents the change from a negative to a positive electrostatic potential, which is mapped onto the electron isodensity surface. Isovalue = 0.001; ESP units: kJ/mol.

optimized geometry of the thiadiazole complex (Figure 2c,d). Under the assumption that these interactions are mainly electrostatic, the interaction energy should gradually increase as the number of nitrogen atoms in the five-membered-ring scaffold increases. However, the energies do not change in the way we expected. Instead, the energy increases by only approximately 1 kcal/mol in going from thiophene to thiazole and then increases dramatically by approximately 4 kcal/mol in going from thiazole to thiadiazole. On the basis of these results, some unknown factors in addition to the electrostatic energy might contribute to the complex formation energy. Thus, separating the total molecular interaction energy into its different components can offer insight into the fundamental nature of the interaction.[47]

3.3. Energy Decomposition Analysis. Energy decomposition analysis (EDA) was performed to determine the components of the interaction energy. The studied complexes were divided into two parts: the sulfur-containing aromatic ring and *N*-methylacetamide. The decomposition analysis of Su and Li[35] was performed using the M06-2X-D3/6-31++G**-optimized structures. The calculated results, which are summarized in Table 3, show that the electrostatic energy (ES), dispersion energy (DISP), and polarization energy (POL) are always favorable for binding between the sulfur-containing aromatic rings and *N*-methylacetamide. Interestingly, although the absolute value of the total interaction energy (E) becomes more favorable as the number of nitrogens in the aromatic ring increases, its components follow different trends. As the number of nitrogens increases, the dipole moment of the sulfur-containing aromatic ring increases (Table S2) and so do the absolute values of ES and POL, while the absolute values of the exchange energy (EX), repulsion energy (REP), and DISP decrease. In addition, the relative contributions of the electrostatic, exchange, polarization, and dispersion energies to the interaction energy vary.

Table 3. Interaction Energy Decomposition Analysis at the M06-2X/6-31++G Level after Application of the BSSE Correction (All Values in kJ/mol)[a]**

	ES	EX	REP	POL	DISP	E
thiophene	−26.8	−24.8	82.7	−7.4	−45.0	−21.4
thiazole-C2	−27.8	−23.0	77.7	−7.6	−41.5	−22.2
thiazole-C5	−28.9	−21.7	71.5	−9.4	−33.3	−21.8
thiadiazole	−33.6	−21.8	72.1	−9.8	−33.1	−26.2

[a]ES, EX, REP, POL, DISP and E denote the electrostatic, exchange, repulsion, polarization, dispersion, and total interaction energies, respectively.

Briefly, the sulfur atoms in functional groups such as sulfhydryl and thioether groups can act as nucleophiles. The QM calculations in this study show that sulfur atoms in aromatic rings can also act as electrophiles and approach other electrophiles in a "side-on" fashion (lateral to the S−C bond). To further explore this type of attraction, a natural bond order (NBO) analysis of thiazole was performed. The configuration of the sulfur atom was found to be $3s^{1.63}\ 3p_x^{1.18}\ 3p_y^{1.58}\ 3p_z^{1.13}$, that is, approximately 92.5% of the six valence electrons occupy the sulfur atomic valence orbitals. This result shows that the S−C bonds are electron-deficient, similar to σ holes. The net natural population analysis (NPA) charge of +0.442 on sulfur also indicates that sulfur is an electrophile in this system.

4. INTERACTION GEOMETRIES AND ENERGY BOUNDARIES

The optimal geometries described previously are not always observed in existing crystal structures because of the interplay of the multiple competing primary and secondary interactions involved in ligand binding. Therefore, the effects of deviations in the S···O distances, σ-hole angles, and spherical angles from their optimal values on the complex formation energy were investigated.

4.1. Distance. In rational drug design, conjugated scaffolds, such as benzene and pyridine, are frequently replaced by sulfur-containing aromatic rings to maintain or increase the binding affinity. The weak C_R−H···O═C hydrogen bond frequently observed for benzene and pyridine rings plays an important role in stabilizing planar conformations of linked heterocyclic systems,[3] particularly in kinase inhibitors. A model system containing a C_R−H···O═C contact, denoted as the "context model" in Figure 4, was employed to calculate a baseline interaction strength. A molecular mechanics distance scan was also performed using the Merck molecular force field (MMFF) for comparison.

Figure 4 shows the dependence of the complex formation energy on the S···O distance. At a distance of 240 pm, the complex formation energy ΔE for the context model was calculated to be −11.5 kJ/mol at the M06-2X-D3/6-31++G** level. This energy is used as a threshold: the introduction of a sulfur atom into the aromatic system needs to be energetically more favorable than −11.5 kJ/mol to improve the binding energy. This threshold leads to different distance ranges in which improved binding is observed for all four sulfur-containing aromatic ligand systems (see Table S3 for details). The curves in Figure 4 reveal that a considerable difference exists between the MMFF method and DFT based results.

Overall, the optimal distance becomes smaller as the number of nitrogens in the ring increases. Deviations from the optimal distance lead to a decrease in the interaction strength. The formation energies of all four model complexes are 50% of their optimal values when the distance is approximately 420 pm or

DOI: 10.1021/acs.jcim.5b00177
J. Chem. Inf. Model. 2015, 55, 2138−2153

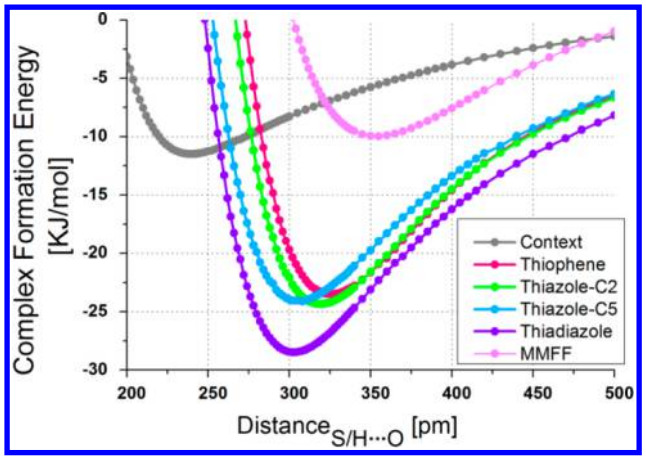

Figure 4. Distance scans for the sulfur-containing aromatic model systems. The complex formation energies of the thiophene, thiazole-C2 (carbonyl oxygen along the C2−S bond direction), thiazole-C5 (carbonyl oxygen along the C5−S bond direction), and thiadiazole complexes are shown as functions of the S···O distance.

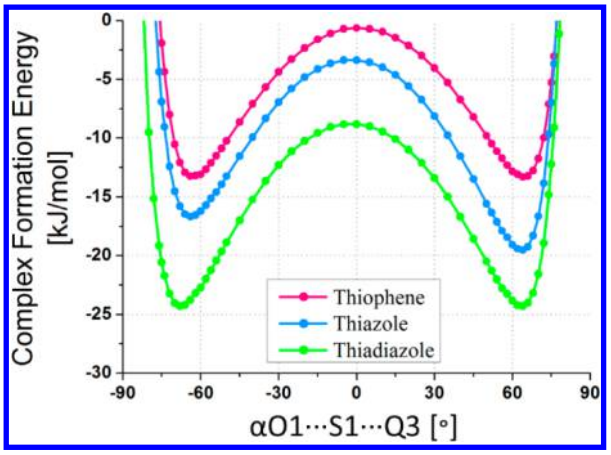

Figure 5. Effect of the σ-hole angle. This graph illustrates the dependence of the complex formation energies of the *N*-methylacetamide and sulfur-containing aromatic model systems on the σ-hole angle: thiophene (pink curve); thiazole (blue curve); thiadiazole (green curve).

the aromatic ring is approximately 42 pm closer to the carbonyl group. Increasing the distance reduces the attractive overlap of the electron-deficient σ hole and the carbonyl lone electron pairs. On the other hand, decreasing the distance increases the repulsive energy between the two molecules. No favorable interactions are observed below 248 pm, indicating that the repulsive forces quickly overcome the attractive interactions when the distance is decreased below the optimum value. As nitrogen atoms are added to the aromatic ring, the interaction distance can be further increased before the interaction energy drops below 50% of its optimal value, and the energy is more favorable than that of the context model over a wider range of distances. The intersection points are particularly useful for scaffold hopping. For thiophene, the distance at which the energy is more favorable than the threshold ranges from 284 to 430 pm, and the largest energy gain relative the context model is 12.0 kJ/mol (at an ideal bond distance of 240 pm). These results explain the multiple occurrences of S···O interactions in the PDB and the increase in affinity reported when furan is substituted by thiophene, as discussed in section 6 describing the QM/MM study. For thiadiazole, the range of distances at which the energy is more favorable than the threshold becomes larger (from 258 to 450 pm), and the energy gain is also larger (17.0 kJ/mol). The two thiazole models have similar ranges of energetically favorable distances (152 pm for the C2−S direction, 156 pm for the C5−S direction) and similar energy gains (12.8 and 12.6 kJ/mol, respectively). Because of the asymmetry of thiazole, two thiazole curves with similar shapes that are slightly translated relative to each other along the *x* axis were obtained. Similar to the results for the optimized conformations, the curve for the C2−S direction follows the thiophene curve, whereas the curve for the C5−S direction follows the thiadiazole curve (Figure 4).

4.2. σ-Hole Angle. To evaluate the effect of the σ-hole angle on the interaction energy, a systematic angle scan was performed, and the results are shown in Figure 5. Two artificial constraints were used in the angle scan, resulting in a difference between the energies of the three constrained complexes and those of the freely optimized complexes. For thiophene, these constraints reduce the strength of the interaction energy the most, by ∼10 kJ/mol. For thiadiazole and thiazole, the interaction energies are reduced by ∼5 and 5−8 kJ/mol, respectively. Interestingly, as the number of nitrogens in the aromatic ring increases, the energy of the geometric constraints decreases. Consequently, these constraints not only avoid the redundant interactions between the aromatic ring and the backbone methyl moiety but also prevent C_R−H···O=C side interactions to some degree, leading to larger differences among the complex formation energies of the three systems obtained from the σ-hole angle scan than among those obtained from the distance scan. For all three systems, the optimal σ-hole angle (α(O···S−C_{ar})) is ∼160° (where α(O_1···S1···Q3) equals ±65°), which is consistent with the QM optimization results, and a significant decrease in the interaction strength is observed when the geometry deviates from the optimal σ-hole angle. In other words, increasing the σ-hole angle by the absolute value of α(O_1···S1···Q3) results in a dramatic decrease in the complex formation energies due to the overlap of the carbonyl oxygen with the hydrogen atom on the aromatic ring. In contrast, decreasing the absolute value of α(O_1···S1···Q3) by 25−35° reduces the energy to 50% of its maximum value. Thus, the Lewis base and the σ hole of the sulfur-containing aromatic molecule cannot interact when the angle deviates 35° from its ideal value, and compounds should be designed to form S···O interactions having a geometry close to the optimal α(O···S−C_{ar}) value (∼160°). This result also confirms the anisotropic nature of S···O interactions.

4.3. Spherical Angles. The degrees of freedom in the spherical orientation of the three aromatic systems were investigated. The obtained interaction spheres for the three sulfur-containing aromatic systems are presented from two different perspectives for the out-of-plane (δ1) rotation (first row in Figure 6) and the in-plane (δ2) rotation (second row in Figure 6). All of the spheres are symmetric with respect to δ1 = 0°. For the in-plane rotation, a strong preference for orientation along the carbon−sulfur bond directions is evident for all three model systems (where δ2 is near ±65°). However, when the absolute value of δ2 is increased by 15°, the energies rapidly become less favorable as a result of steric hindrance. The in-plane spherical scan results are consistent with those of the σ-hole angle scan. For the out-of-plane spherical scan, the energy strongly depends on δ1 when δ2 is approximately ±65°. For thiophene, strong interactions are observed (the area remains

DOI: 10.1021/acs.jcim.5b00177
J. Chem. Inf. Model. 2015, 55, 2138−2153

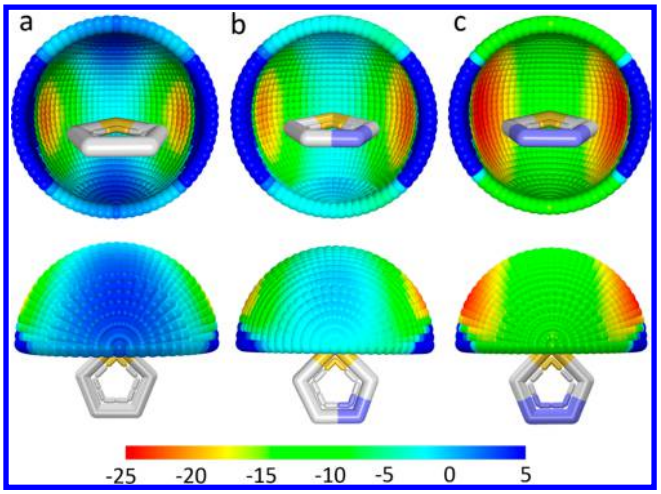

Figure 6. Spherical scan plots for the backbone and sulfur-containing aromatic ring model systems showing the interaction energy spheres for the (a) thiophene−backbone, (b) thiazole−backbone, and (c) thiadiazole−backbone complexes. The color gradient from red to blue indicates a decrease in the strength of the complex interactions, that is, a change in the conformation energy from −25 to 5 kJ/mol.

orange) for $\delta 1$ values of ±30° from the 0° geometry. For thiazole, the interactions on both sides of the sulfur are stronger (redder) than those observed for thiophene. However, the σ hole near the nitrogen is larger than that on the other side of the ring; when $\delta 1$ varies within ±40° of the C2−S bond direction, strong interactions are observed, whereas the range of strong interactions increases to ±50° for interactions centered along the C5−S bond direction. For thiadiazole, strong interactions are observed when $\delta 1$ varies by up to ±60° from the 0° geometry. Overall, the areas with high interaction energies, denoted as hot areas (red or orange areas in Figure 6), are consistent with the shapes of the σ holes on the ESP surfaces (Figure 3), which indicate relatively positive areas on the aromatic rings caused by the anisotropic electron density distribution on the sulfur atom. Therefore, the interaction strength largely depends on the orientation of the electronegative interaction partner as it approaches the electron-deficient areas on the sulfur-containing aromatic ligands.

4.4. Interdependence of the S···O Distance and σ-Hole Angle. In the previous sections, the different degrees of freedom (S···O distance, σ-hole angle, spherical angles) were explored separately. Here, the interdependence of the effects of the S···O distance and σ-hole angle on the formation energy are discussed. In these calculations, the spherical angles were fixed for simplicity. The results for the thiazole and thiophene model systems are presented in Figure 7. It was assumed that interaction hot spots are centered at a S···O distance of 300−350 pm and $\alpha(O_1\cdots S1\cdots Q3)$ of 60°−70° on the basis of the spherical scans (Figure 6) and the ESP surfaces of the three scaffolds (Figure 3). However, the hot spots (red to yellow color gradient) are slim and tilted, as shown in Figure 7. For the thiophene system, the energies in the hot spot, which is defined by a S···O distance range of 280−460 pm and $\alpha(O_1\cdots S1\cdots Q3)$ range of 60−90°, are among the top 30% of the largest favorable energies. Below 30°, all of the interaction energies are less favorable (areas colored cyan and blue represent energies higher than −5 kJ/mol). For the thiazole system, the σ hole in the C2−S bond direction is wider and has stronger interactions (is redder) than that in the C5−S bond direction (the angle of the former is positive, whereas the latter is negative). The top 25% of the largest interaction energies are observed for geometries with S···O distances between 270 and 450 pm and optimal σ-hole angles between 60° and 90° (or −60° and −90°). These results can be explained by multiple hydrogen and sulfur contributions to the σ holes. When the S···O distance is within 370 pm, the hot spots are located along the C−S bond direction; thus, sulfur is the major contributor to the positive potential area. If the distance is greater than 370 pm, the hydrogen contribution increases, and the hot spots shift to 90° near the hydrogen. Intriguingly, these various forces lead to an hourglass-shaped cyan and blue area in the two-dimensional (2D) projection for the thiazole model system (Figure 8). In the following sections, these two plots are used to analyze the sulfur−oxygen geometric statistics extracted from the PDB.

5. COMPARISON OF THEORETICAL AND EXPERIMENTAL DATA

5.1. General Considerations. Structural information obtained from the PDB has been widely used to derive scoring functions and to characterize the optimal geometries of various

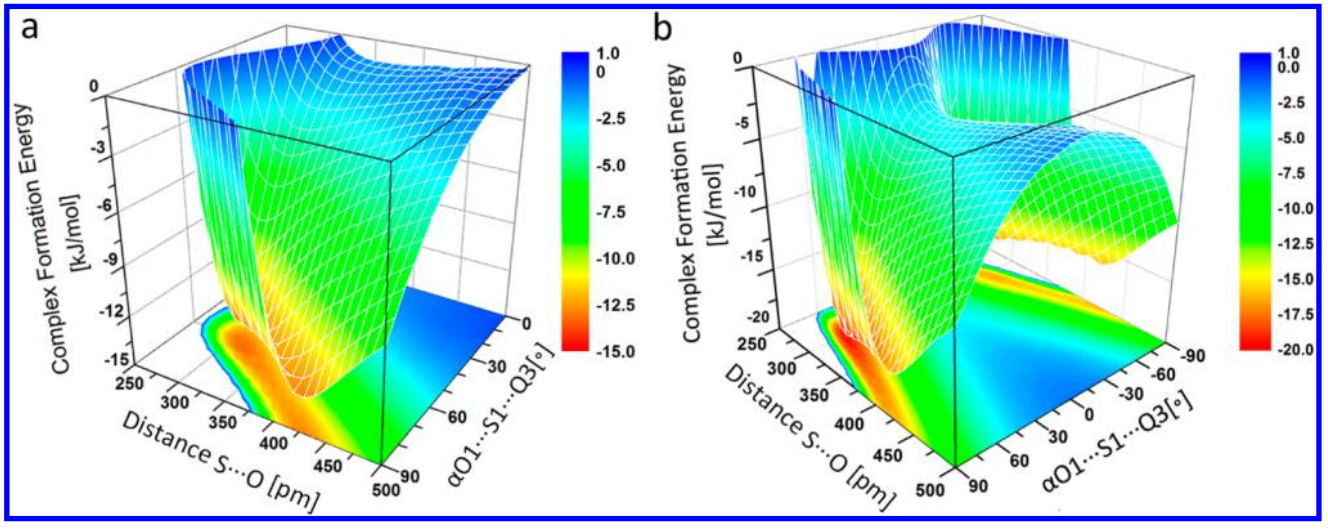

Figure 7. Interdependence of the S···O distance and σ-hole angle for the (a) thiophene−backbone and (b) thiazole−backbone model systems.

DOI: 10.1021/acs.jcim.5b00177
J. Chem. Inf. Model. 2015, 55, 2138−2153

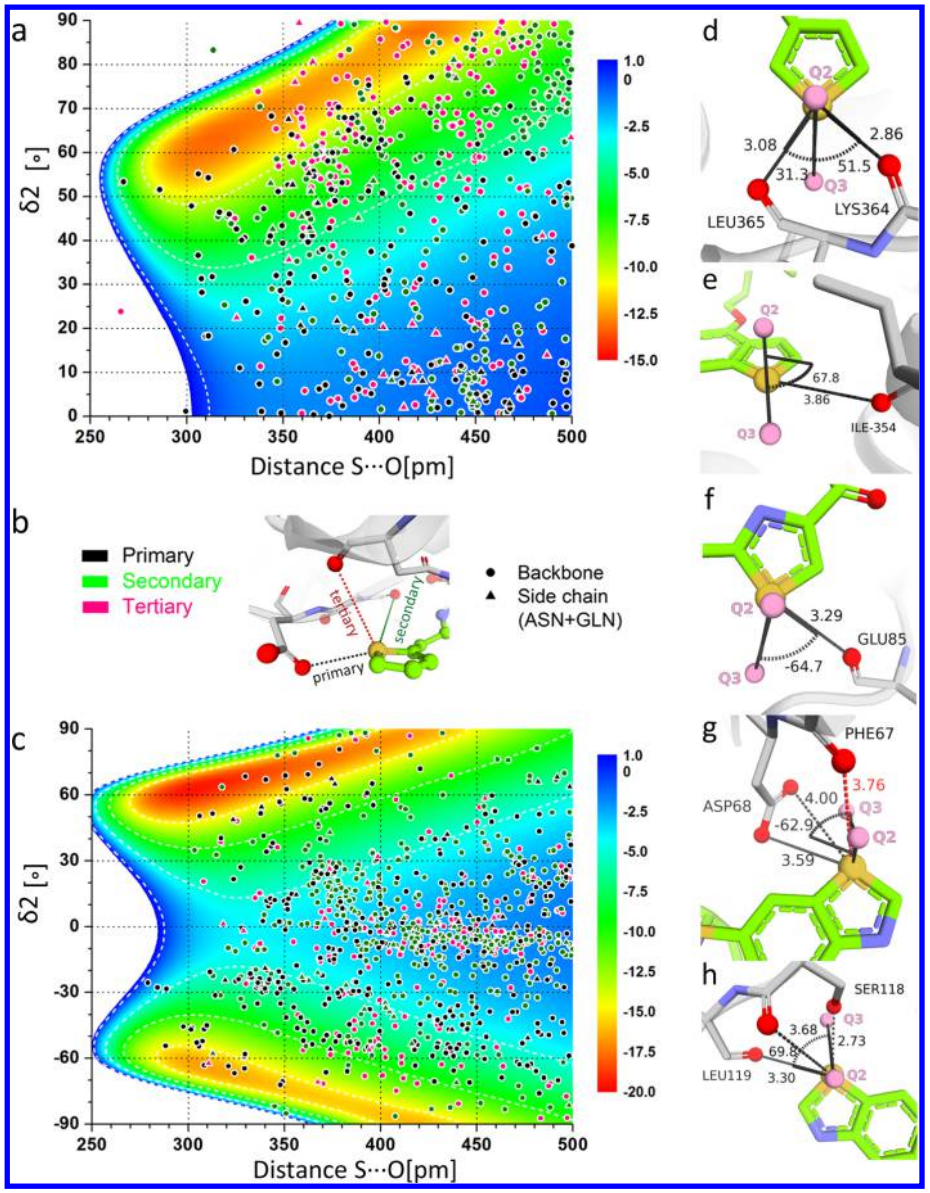

Figure 8. (a, c) Mappings of the overall PDB statistics onto the 2D distance−angle scans for the (a) thiophene and (c) thiazole model systems. (b) The interaction hierarchy is represented by different colors and symbols: primary contact (black), secondary contact (green), and tertiary contact (pink). The carbonyl oxygens are classified into two subcategories: backbone (circles) and side chain (triangles). (d−h) Representative examples of sulfur−oxygen interactions involving backbone carbonyl oxygens, with the following PDB codes: (d) 3FUN (LTA4H); (e) 3G8I (PPAR-α/γ); (f) 3U9N (CHK1/CDK2); (g, h) 4JFJ (FKBP51). The acronyms in parentheses are the targets for each protein. The ligands and the residues that interact with them are shown as sticks (carbon, green for ligands and silver for proteins; oxygen, red; nitrogen, blue; sulfur, yellow). The thiophene or thiazole sulfur atom, the oxygen atoms with which it interacts (within 500 pm of sulfur) and the dummy atoms Q2 and Q3 are represented as balls. The protein is shown as a cartoon. The S···O contacts are shown in black, and the hydrogen bonds are shown in yellow. These conventions are also used in Figure 10.

intermolecular interactions; thus, it is also valuable for determining the areas of the 2D sulfur−oxygen interaction energy projections that are preferentially populated under experimental conditions. All of the contacts between sulfur atoms in aromatic rings and oxygen atoms in protein residues were extracted from a recent version of the PDB. The oxygens that interact with sulfur were divided into three categories: (a) carbonyl oxygens in protein backbones or in the asparagine or glutamine side chains; (b) hydroxyl oxygens in serine, threonine, or tyrosine; and (c) carboxyl oxygens in aspartate or glutamate. Some constraints of this analysis method should be noted:

(1) The 2D heat maps are based on small model systems, meaning they do not account for the impact of different scaffolds (e.g., benzothiazole, thienopyrimidine, and thienopyrazole) and substituents (e.g., fluorine, hydroxyl, and amino groups) on the sulfur-containing aromatic rings or for various polarization effects on the carbonyl oxygen in the protein binding site.
(2) Thermodynamic factors, such as solvation, conformational changes, and entropic terms, were neglected in the binding free energy calculations. Thus, the "strength" of an interaction is not the real strength in binding.
(3) The angle at which the carbonyl group approaches the σ hole has been studied in detail by Iwaoka et al.[11]

DOI: 10.1021/acs.jcim.5b00177
J. Chem. Inf. Model. 2015, 55, 2138−2153

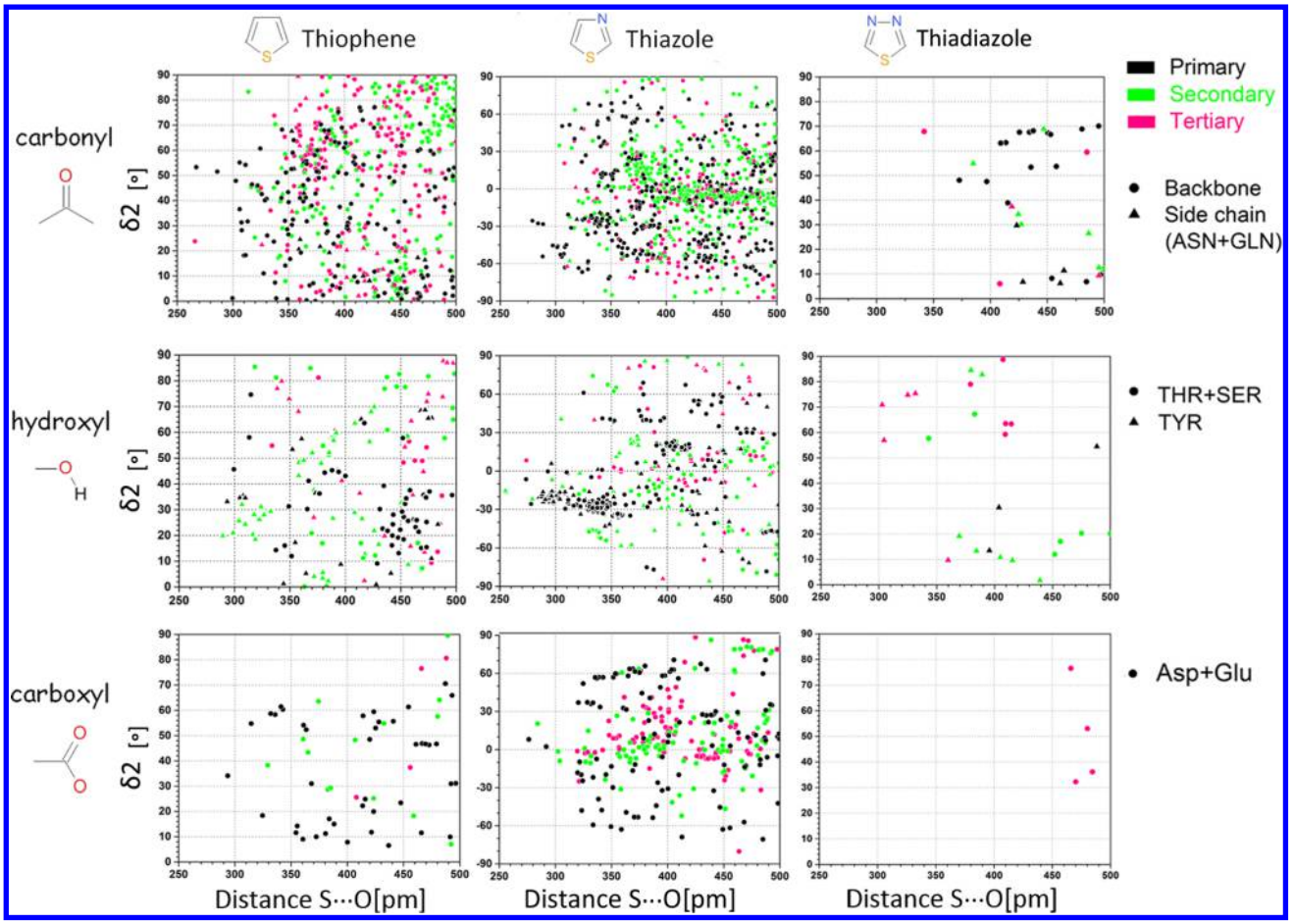

Figure 9. PDB mining results for intermolecular S···O contacts.

According to their research, both the π_O and σ_O directions of the carbonyl oxygen are preferable. Thus, the influence of the carbonyl oxygen orientation on the interaction strength was ignored.

(4) The S···O interactions are classified as primary, secondary, and tertiary on the basis of the spherical angles. Three different contacts are shown in detail in Figure 8b (PDB code 1YM1[48]) to better illustrate the hierarchy.

In real biological systems, ligands and proteins usually interact via multiple contacts. As a result, even if all of the above factors were included in the assessment, a thorough understanding of the specific molecular interactions in these systems would not be obtained because of their nonadditive nature, which holds whether or not they are the same type of interaction. Additionally, the crystal structures in the PDB are static and might not represent the optimal conformations in the real system. Therefore, all of these limitations indicate that the comparison of the model calculations to the statistical analysis serves only as a rough guideline for illustrating the geometries of interacting species and deriving scoring functions for medicinal and computational chemists. Because of the many S···O contacts found in this PDB analysis, the structures were categorized on the basis of the type of side chain or backbone oxygen participating in the interaction. For each category, representative examples are presented.

The frequencies of the S···O interactions involving the three sulfur-containing aromatic rings in the PDB follow the order thiadiazole < thiophene < thiazole (Figure 9). The ratio of thiophene S···O contacts to thiadiazole S···O contacts (13:1) is similar to the ratio of the total numbers of their structures in the PDB (16:1). However, the ratio of the thiazole S···O contacts to thiophene S···O contacts (2:1) is twice that of the total numbers of their structures in the PDB (1:1). All three types of interactions are found to be evenly distributed in the hot and green areas. However, many contacts are clustered in the hot areas according to the PDB analysis, suggesting that these contacts are nearly optimal interactions (Figure 8d–h). Of the different types of oxygen atoms participating in the interactions, backbone carbonyl oxygens are observed to interact with sulfur most frequently. Nonetheless, in addition to the structural constraints of the ligands and proteins, competition with water, ions, and hydrogen-bond donors and acceptors limits the number of effective targetable S···O contacts, and many secondary and tertiary interactions are observed.

5.2. Targeting of Backbone Carbonyls. *5.2.1. Thiophene.* Backbone carbonyl oxygens are the primary S···O contact acceptors in proteins. Only three complexes between proteins and ligands containing thiophene have unfavorable interaction energies (white segments in Figure 8a). For thiophene-containing ligands in general, longer S···O distances and smaller σ-hole angles are frequently observed. The backbone carbonyl groups are categorized into three subclasses on the basis of their locations in the protein: in the loop regions, α-helices, and β-sheets. These groups are fundamental units of proteins, and each one has a different degree of

DOI: 10.1021/acs.jcim.5b00177
J. Chem. Inf. Model. 2015, 55, 2138–2153

Chart 1. Structures Used in the Case Studies

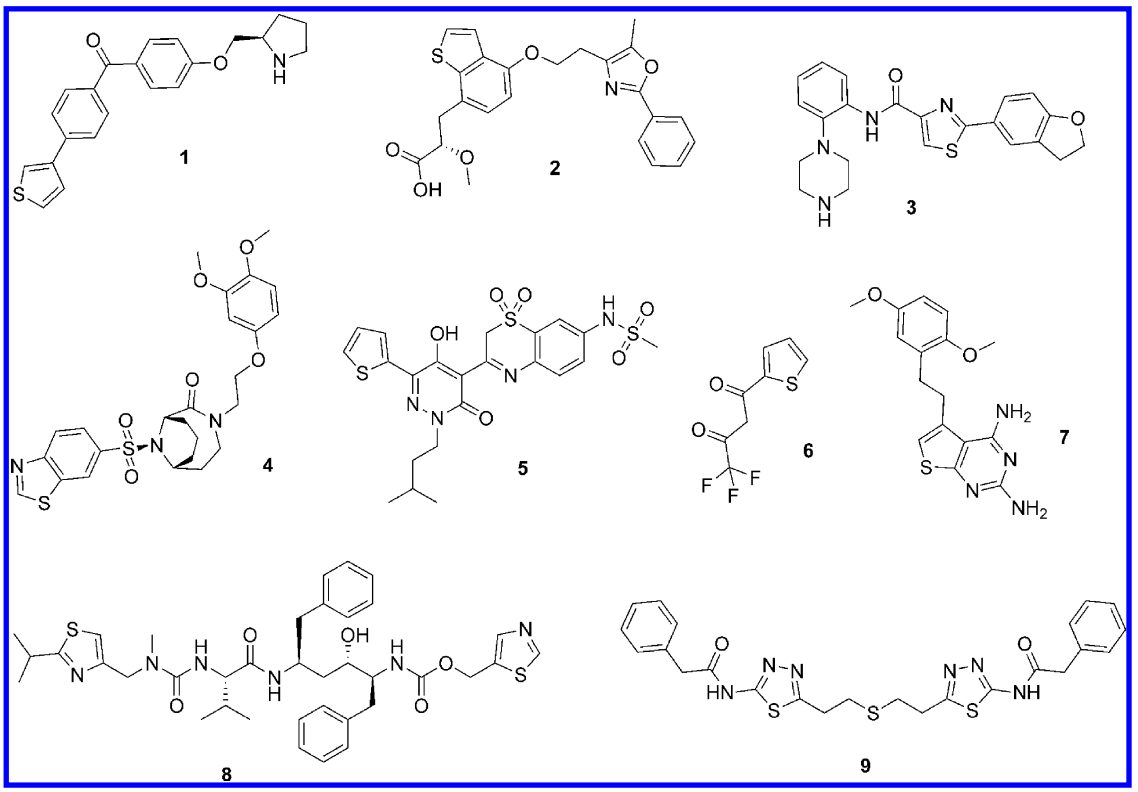

freedom. Two representative examples of carbonyl oxygens, one in a loop and the other in an α-helix, are discussed below.

The first interesting example is a bifurcated S···O contact within the hinge binding motif in leukotriene A4 hydrolase (LTA4H). The {4-[(2*R*)-pyrrolidin-2-ylmethoxy]phenyl}(4-thiophen-3-ylphenyl)methanone fragment (**1**) (Chart 1) was shown to be a potent LTA4H inhibitor with an IC_{50} value of 189 nM via a hydrolase assay.[49] A suboptimal interaction and a weak interaction between the thiophene sulfur and the carbonyl oxygens of Lys364 ($d_{S\cdots O}$ = 286 pm, σ-hole angle = 51.5°, primary) and Leu365 ($d_{S\cdots O}$ = 308 pm, σ-hole angle = 31.3°, primary), respectively, are found within the deep LTA4H active-site pocket. These two interactions fix the sulfur atom between the carbonyl oxygens, explaining the high activity of this fragment (PDB code 3FUN;[49] Figure 8d).

In another example, the thiophene sulfur interacts with a backbone carbonyl oxygen in an α-helix. When cocrystallized with PPAR-α (PDB code 3G8I;[50] Figure 8e), aleglitazar (**2**) (Chart 1), a potent and balanced dual peroxisome proliferator-activated receptor (PPAR) α/γ agonist (IC_{50} = 38 nM for PPAR-α, 19 nM for PPAR-γ) used to treat type II diabetes,[50] forms a suboptimal interaction with the Ile354 carbonyl oxygen ($d_{S\cdots O}$ = 386 pm, σ-hole angle = 67.8°, primary) and four strong hydrogen bonds with PPAR-α through the acidic warhead. Because the Ile354 carbonyl oxygen on the α-helix forms a strong hydrogen bond with the Lys358 amino nitrogen, it has less flexibility than the carbonyl oxygen in the loop region, leading to a slightly suboptimal conformation of the sulfur−oxygen interaction.

5.2.2. Thiazole. The PDB analysis shows that many thiazole-containing compounds form S···O contacts within the energy hot spots, indicating that the interactions are nearly optimal. Clusters of secondary and tertiary contacts are also observed in regions with very weak complex formation energies (blue segments in Figure 8c), which might be the result of polymers. Three distinct ligands with thiazole rings form suitable S···O contacts with carbonyl oxygens in the loop region and in α-helices.

A very nice example of a S···O contact with a distinctive hinge binding motif is observed for the novel checkpoint kinase 1 (CHK1) inhibitor 2-(2,3-dihydro-1-benzofuran-5-yl)-*N*-(2-piperazin-1-ylphenyl)-1,3-thiazole-4-carboxamide (**3**) (Chart 1). When used as an ATP agonist, **3** has apparent IC_{50} values of 75 nM (CHK1) and 2.7 nM (cyclin-dependent kinase 2 (CDK2)).[51] The thiazole sulfur of **3** interacts with the Glu85 main-chain carbonyl oxygen in the hinge region, which is exposed to the binding site (PDB code 3U9N;[51] Figure 8f) in an ideal orientation ($d_{S\cdots O}$ = 329 pm, σ-hole angle = −64.6°). This structure is the first reported example in which a kinase forms this unusual sulfur−oxygen interaction with a thiazole sulfur atom.

Another interesting contact is observed between FK506-binding protein 51 (FKBP51) and the binder (1*R*,6*S*,10*R*)-10-(1,3-benzothiazol-6-ylsulfonyl)-4-[2-(3,4-dimethoxyphenoxy)-ethyl]-4,10-diazabicyclo[4.3.1]decan-5-one (**4**) (Chart 1) (K_i = 2100 nM).[52] The binder is bound to the protein in two different configurations (PDB code 4JFJ;[52] Figure 8g,h). In one of the configurations, the benzothiazole substituent forms an optimal contact with the Leu119 carbonyl oxygen ($d_{S\cdots O}$ = 330 pm, σ-hole angle = 68.3°) and two weak interactions with the carbonyl and hydroxyl oxygens of Ser118 (OH: $d_{S\cdots O}$ = 274 pm, σ-hole angle = −6.4°, primary; C═O: $d_{S\cdots O}$ = 368 pm, σ-hole angle = 45.3°, secondary), which is located in a loop region (Figure 8g). If the terminal benzothiazole is rotated 180°, it interacts with both carboxyl oxygens of Asp68 ($d_{S\cdots O}$ = 359 pm, σ-hole angle = −62.9°; $d_{S\cdots O}$ = 400 pm, σ-hole angle = −30.9°) and forms a tertiary contact with the Phe67 carbonyl oxygen ($d_{S\cdots O}$ = 376 pm, σ-hole angle = −3.0°), which is located in a β-

DOI: 10.1021/acs.jcim.5b00177
J. Chem. Inf. Model. 2015, 55, 2138−2153

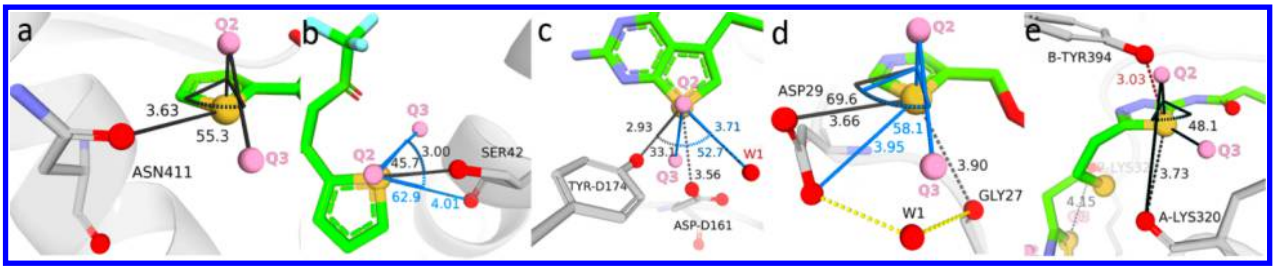

Figure 10. Representative examples of sulfur−oxygen interactions involving side-chain oxygens, with the following PDB codes: (a) 3CWJ (HCV NS5B); (b) 1ZP0 (SQR); (c) 3MCV (TbPTR1); (d) 4EYR (HIV-1 protease); (e) 3UO9 (GAC). Some of these contacts are shown in blue to differentiate them.

sheet (Figure 8h). Because the carboxyl oxygen is a stronger Lewis base than the carbonyl oxygen, targeting the negatively charged aspartate should lead to a stronger S···O interaction. Thus, the occupancy of the second state is indeed more likely (first vs second state: 0.2 vs 0.4).

Overall, carbonyl oxygens in loop regions have more degrees of freedom than those in α-helices and β-sheets, as demonstrated by the above case studies. S···O interactions involving carbonyl oxygens in the loop region are observed most frequently, and these oxygens tend to form multiple S···O interactions. Because the strength of a S···O interaction is equal to that of a typical hydrogen bond, the common bifurcated and trifurcated S···O interactions are stronger and more likely to improve the binding affinity without requiring additional desolvation. In some cases, a substituent (e.g., 2-amino) on thiophene or thiazole can aid in the formation of a network of interactions, leading to high biological activity.

5.3. Targeting of Side Chains. *5.3.1. Targeting of Side-Chain Carbonyls.* Numerous examples of amino carbonyl groups on asparagine or glutamine side chains forming favorable S···O interactions with thiophene exist. Two specific examples of this type of interaction are discussed below. The compound *N*-[3-[5-hydroxy-2-(3-methylbutyl)-3-oxo-6-thiophen-2-ylpyridazin-4-yl]-1,1-dioxo-2*H*-benzo[*b*][1,4]thiazin-7-yl]methanesulfonamide (**5**) (Chart 1) has been shown to be a potent inhibitor of HCV NS5B polymerase (IC_{50} 1b < 10 nM, EC_{50} 1b = 1.1 nM, where 1b denotes the genotype 1b assay).[53] The sulfur atom of the terminal thiophene ring forms a primary contact with the Asn411 amino carbonyl oxygen (on chain A: $d_{S\cdots O}$ = 363 pm, σ-hole angle = 52.3°; on chain B: $d_{S\cdots O}$ = 355 pm, σ-hole angle = 52.7°) (PDB code 3CWJ;[53] Figure 10a).

5.3.2. Targeting of Hydroxyl Oxygens on Serine and Threonine. In theory, hydroxyl oxygens have more degrees of freedom than backbone carbonyl oxygens and should form stronger S···O interactions. However, because hydroxyl groups can act as hydrogen-bond acceptors and donors, the sulfur-containing aromatic rings must compete with other polymer, solvent, and cationic hydrogen-bond donors and acceptors. As a result, only a few optimal S···O contacts between thiophene or thiazole sulfurs and hydroxyl oxygens have been observed, despite the fact that numerous contacts of this type exist.

2-Thenoyltrifluoroacetone (TTFA, **6**) (Chart 1) inhibits ubiquinone reduction by ubiquinone oxidoreductase (SQR) by occupying the ubiquinone binding site (PDB code 1ZP0;[54] Figure 10b). The thenoyl sulfur atom interacts with the hydroxyl and carbonyl oxygens of Ser-C42 (OH: $d_{S\cdots O}$ = 300 pm, σ-hole angle = 45.7°, primary; C═O: $d_{S\cdots O}$ = 401 pm, σ-hole angle = 62.9°, primary), which is located on an α-helix. Because the Ser-C42 carbonyl oxygen participates in the hydrogen bonds that stabilize the helix, the geometry of its interaction with sulfur deviates from the optimal interaction geometry. However, the hydroxyl oxygen on the side chain has more degrees of freedom than the carbonyl group, and thus, its interaction with sulfur is more favorable.

5.3.3. Targeting of Hydroxyl Oxygens on Tyrosine. In the case of tyrosine, both its oxygen atom and π electrons can interact with sulfur-containing aromatic rings. Thus, placing thiophene or thiazole in a pocket that contains tyrosine can increase the ligand−protein interactions in multiple dimensions. The following example demonstrates these multiple interactions.

5-[2-(2,5-Dimethoxyphenyl)ethyl]thieno[2,3-*d*]pyrimidine-2,4-diamine (**7**) (Chart 1) inhibits *Trypanosoma brucei* pteridine reductase (TbPTR1) ($K_i \approx 70$ nM).[55] The benzothiophene sulfur atom forms two primary sulfur−oxygen interactions with the hydroxyl oxygens of Tyr174 and water W1. A vertical $\pi-\pi$ interaction is also formed between Tyr174 and the benzothiophene rings (PDB code 3MCV;[55] Figure 10c). Intriguingly, the water participates in a network of hydrogen-bonded solvent molecules near Asp161. The binding modes of all four monomers of the TbPTR1−**7** complex are similar.

5.3.4. Targeting of Carboxyl Groups. The negatively charged aspartate and glutamate residues are stronger Lewis bases than carbonyl and hydroxyl oxygens. Theoretically, they should participate in stronger S···O interactions. The two electronically identical oxygens in the carboxyl group can interact with one sulfur atom simultaneously, and bifurcated or trifurcated interactions are very common on the basis of the PDB mining results.

The cocrystal of ritonavir (RTV) and HIV-1 protease has a bifurcated contact. RTV (**8**) (Chart 1) is a first-generation HIV-1 protease inhibitor to which drug resistance is rapidly emerging.[56] It has two thiazole rings: one with an isopropyl group and one without this substituent. The former thiazole ring occupies a pocket, preventing the sulfur from forming a strong contact with an oxygen, whereas the latter thiazole forms three sulfur−oxygen interactions with two residues (PDB code 4EYR;[56] Figure 10d). Specifically, the thiazole sulfur forms two optimal primary contacts with the Asp29 carboxyl oxygens ($d_{S\cdots O}$ = 366 pm, σ-hole angle = 63.5°; $d_{S\cdots O}$ = 395 pm, σ-hole angle = 58.1°) and a secondary contact with the Gly27 carbonyl oxygen ($d_{S\cdots O}$ = 399 pm, σ-hole angle = 50.0°). Because Gly27 also participates in a water bridge to the Asp29 carboxyl groups, this sulfur−oxygen interaction deviates from the optimal geometry.

5.4. Thiadiazole−Oxygen Interactions. Very few S···O contacts involving thiadiazole scaffolds were found in the PDB. This low frequency is expected in view of the fact that the number of thiadiazole-containing ligands is less than 100.

DOI: 10.1021/acs.jcim.5b00177
J. Chem. Inf. Model. 2015, 55, 2138−2153

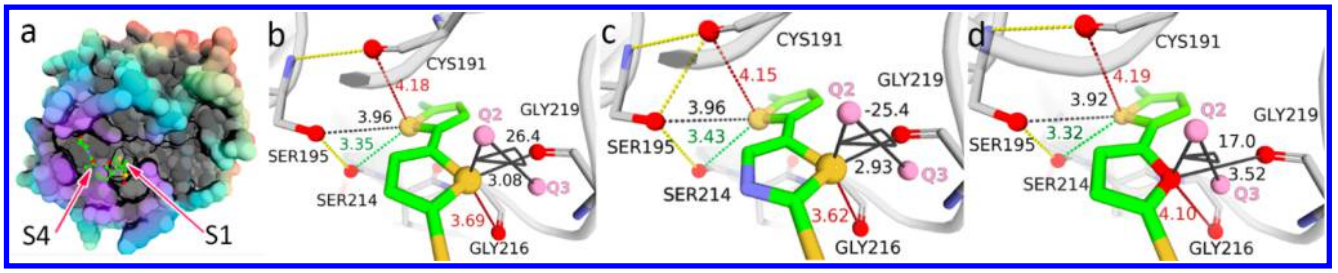

Figure 11. (a) Schematic surface representation of FXa (PDB code 2J95) with a thiophene-containing inhibitor. (b–d) Optimized structures of the complexes of (b) **10**, (c) **11**, and (d) **12** with FXa. Atoms in the QM layer are shown as sticks, and atoms in the MM layer are shown as a cartoon. The protein surface is colored on the basis of its distance from the ligand; the color changes from violet to red with increasing root-mean-square deviation from the ligand.

Chart 2. Structures Used in the QM/MM Study

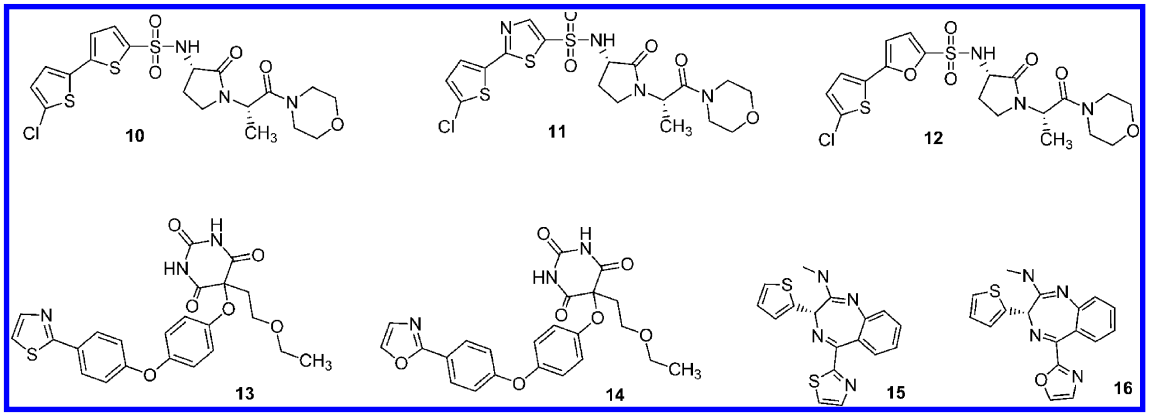

Although thiadiazole forms the strongest S···O interactions (as shown in Table 1), only a few oxygen atoms form S···O contacts with it. Nevertheless, two representative examples are described below.

Bis[2-(5-phenylacetamido-1,3,4-thiadiazol-2-yl)ethyl] sulfide (BPTES, **9**) (Chart 1) selectively inhibits GLS1 (glutaminase) activity over GLS2 activity by locking GLS1 into a nonproductive state (IC_{50} = 60 nM for GLS1). The BPTES molecule binds at the short dimer–dimer interface of human GAC's inactive conformation (PDB code 3UO9[57]). The thiadiazole sulfur atom interacts with Lys320 in the loop region and Tyr394 in the interface helix as shown in Figure 10e. Tyr395 appears to contribute to the binding by forming a π–π stacking interaction with BPTES instead of a S···O contact. In addition, the thiadiazolyl amide nitrogen atoms form a series of hydrogen bonds with backbone atoms. All of these interactions with the tetramer residues occur in a highly symmetric fashion, indicating that allosteric inhibition occurs via tetramer stabilization.

5.5. Brief Summary of the Case Studies. On the basis of the observed optimal S···O interactions, the ability of sulfur-containing aromatic rings to form multiple interactions is their main advantage. First, Lewis bases can approach the sulfur atom on each of the three scaffolds from two different directions. Second, the aromatic rings also have π electrons that can interact with phenyl and histidine rings. Third, even Lewis bases that cannot form optimal interactions with the sulfur atom can polarize it to improve the strength of suboptimal S···O interactions. On the basis of the above analyses, thiophene, thiazole, and thiadiazole are useful scaffolds for replacing water or forming a complex network of polar interactions. Moreover, these three ring systems, especially thiophene and thiazole, are employed as binding agents for a diverse set of medicinally relevant proteins that exhibit a wide variety of biological activities, such as antibiotics, antiviral agents, central nervous system drugs, hypoglycemic agents, antineoplastic agents, anti-inflammatory agents, etc. When these ring systems contribute to a network of polar contacts between the ligand and protein, high binding affinity is usually observed in biological experiments. This work thus provides novel strategies for replacing water and forming networks of polar contacts for chemists working in rational drug design.

6. QM/MM STUDY OF SULFUR–OXYGEN INTERACTIONS IN PROTEIN–LIGAND COMPLEXES

To better understand the effects of sulfur–oxygen interactions on biological systems, we modeled protein–ligand complexes from the PDB that contain sulfur–oxygen interactions and have reported biological activities. Three crystal structures of sulfur-containing ligands (pyrimidinetrione, pyridodiazepineamine, and a sulfonamide derivative) with their corresponding proteins (PDB entries 2J95,[58] 1YOU,[59] and 2W4I[60]) were selected for the QM/MM calculations. Because these particular sulfur–oxygen contacts have not been parametrized in current molecular mechanics force fields, the unique combined QM/MM method is suitable for estimating the S···O interactions at a reasonable computational cost.[61−64] The corresponding complexes in which the sulfur-containing rings were replaced by non-sulfur-containing rings (i.e., oxazole, furan) were also investigated for comparison.

6.1. Factor Xa Inhibitors. The dysregulation of activated factor X (FXa) formation is a key driver of thrombosis, which can develop into ischemia and cause life-threatening conditions such as myocardial infarctions and strokes. Therefore, thrombin and FXa are attractive targets for pharmacological thrombosis

DOI: 10.1021/acs.jcim.5b00177
J. Chem. Inf. Model. 2015, 55, 2138–2153

Table 4. Comparison of the Experimental Binding Affinities and Results of QM/MM Calculations

	10	11	12	13	14	15	16
biological activity (nM)[a]	4	5	1200	3.6 (150)	18 (360)	1700	7700
$\Delta\Delta E$ (kJ/mol)[b]	−27.90	−27.93	0.0	−37.7	0.0	−13.4	0.0

[a]For **10**–**12**, the biological activity is the K_i of FXa. For **13** and **14**, the biological activities are IC_{50} of MMP-13 (MMP-14). For **15** and **16**, the biological activity is IC_{50} of *H. pylori* MurI. [b]$\Delta\Delta E$ values are given relative to the compound with the furan or oxazole ring for each series.

intervention. Chan et al.[58] identified efficacious oral FXa inhibitors containing a 3-aminopyrrolidin-2-one scaffold. The morpholino amide occupies the aromatic box of the S4 pocket, whereas the chloroaromatic P1 substituents bind to the highly electron-rich S1 pocket (Figure 11a), which indicates that the positive σ holes on the sulfur are desirable, as shown by the QM/MM calculations and experimental data. According to the QM/MM calculations, the interaction energies for the thiophene and thiazole ligands (**10** and **11**, respectively; Chart 2) are 27.9 kJ/mol lower than that for the furan ligand (**12**; Chart 2), and the sulfur-containing ligands improve the inhibitory activity by 3 orders of magnitude relative to the furan ligand (from ∼5 to 1200 nM; Table 4). In the S1 pocket, the terminal chlorothienyl groups of the three compounds form similar S···O interactions with three oxygen atoms, stabilizing the ligand conformation (Figure 11b–d). However, the proximal sulfur-containing aromatic rings interact with the carbonyl oxygens of Gly216 and Gly219 in the flexible loop. The S···O distances for the thiophene and thiazole analogues are much shorter (Figure 11b,c) than the O···O distance for **12** (Figure 11d), indicating that the oxygen atoms are attracted by the sulfur atoms. The primary contacts between the Gly219 oxygen and the sulfur atoms are strong, whereas the contacts between the Gly216 oxygen and the sulfur atoms are weaker tertiary contacts. These QM/MM interaction energies are larger (up to 27 kJ/mol) than those of the model systems in the previous sections, which can be attributed to the increased polarization of sulfur by electron-withdrawing sulfonamides. In summary, this example illustrates a successful aromatic scaffold substitution in drug development.

6.2. Selective MMP Inhibitors. Matrix metalloproteinase (MMP) inhibitors are therapeutically useful for curing osteoarthritis (OA). Blagg et al.[59] attempted to discover an MMP-13 inhibitor that does not inhibit MMP-14 because MMP-13 plays a critical role in OA pathology, whereas MMP-14 is possibly the main reason for musculoskeletal side effects. The pyrimidinetrione core of the discovered inhibitor occupies the deep, narrow S1′ pocket of MMP-13 to bind to zinc (Figure 12a), and optimizing the C4 substituent of the terminal aromatic ring can make the inhibitor selective for MMP-13. According to the QM/MM calculations, replacing the thiazole ring in **13** (Chart 2) with the oxazole ring in **14** (Chart 2) leads to a loss of 38 kJ/mol in the interaction energy (Table 4). Notably, this energy is significantly larger than the energy of a typical S···O interaction on an absolute scale. Analysis of the QM/MM-optimized protein–ligand complex reveals that this large interaction energy might be due to multiple interactions between sulfur and carbonyl oxygen atoms in the binding pocket. Although the Thr245 hydroxyl oxygen and Pro276 carbonyl oxygen form tertiary and secondary sulfur–oxygen contacts, respectively (Figure 12b), they might contribute approximately −5 kJ/mol to the interaction energy on the basis of the 2D heat map in Figure 8c. For the oxazole ligand, the electron-rich carbonyl oxygen of Gly273 interacts repulsively with the oxazole oxygen, which is at a distance of 283 pm

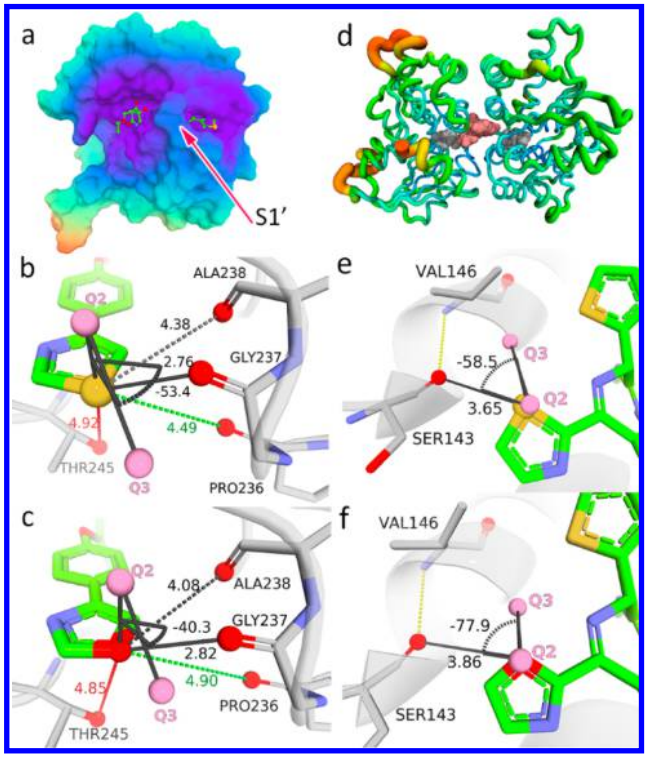

Figure 12. (a) Schematic surface representation of the MMP-13 catalytic domain (PDB code 1YOU). (b, c) Optimized structures of the complexes of (b) **13** and (c) **14** with MMP-13. (d) Structure of a pyridodiazepineamine with a thiazole moiety (shown as pink spheres) binding at the MurI enzyme dimer interface (presented as a cartoon colored by the b-factor) (PDB code 2W4I). (e, f) Optimized structures of the complexes of (e) **15** and (f) **16** with MurI.

(Figure 12c). In contrast, for the thiazole ligand, the orientation of the Gly273 carbonyl oxygen and its distance from the sulfur atom indicates that a primary S···O contact is formed (Figure 12b). The interaction energy could be as large as −20 kJ/mol on the basis of the previous 2D projection scan (Figure 8c). Moreover, an increase in the MMP-13 selectivity is also observed when **13** is substituted for **14**; the ratio of the MMP14 and MMP-13 IC_{50} values increases from 2.4 to 5.0 (Table 4). Therefore, in this case the sulfur–oxygen interaction not only increases the biological activity but also improves the selectivity.

6.3. Selective *Helicobacter pylori* Glutamate Racemase (MurI) Inhibitors. *Helicobacter pylori* infections can cause chronic peptic ulceration and increase the risk of gastric adenocarcinoma. MurI is a bacterial cytoplasmic enzyme that catalyzes the conversion of L-glutamate to D-glutamate; the latter is an essential amino acid in the peptidoglycan synthesis of bacterial cell walls. Interestingly, *H. pylori* MurI has unique biophysical and biochemical properties compared to MurI of other bacteria. Thus, the discovery and development of specific MurI inhibitors can reduce disturbances to commensal bacteria in the gastrointestinal (GI) tract, reduce resistance, and

DOI: 10.1021/acs.jcim.5b00177
J. Chem. Inf. Model. 2015, 55, 2138–2153

improve patient compliance. Benzodiazepineamines, which Geng et al.[60] identified by high-throughput screening, have proven to be highly selective against *H. pylori* MurI. The two molecules selected for the QM/MM study each have two five-membered rings, thiophene and thiazole for compound **15** (Chart 2) and thiophene and oxazole for **16** (Chart 2). For **15**, the thiazole sulfur atom is within 500 pm of a carbonyl oxygen atom (Ser143). However, the Ser143 carbonyl oxygen is on the MurI α-helix and forms a hydrogen bond to the adjacent residue (Val146) to stabilize the α-helix (Figure 12d). These interactions reduce the flexibility of these two residues, as confirmed by the QM/MM calculations and the activity data. For **16**, the Ser143 carbonyl oxygen is repulsed by the oxazole oxygen and instead forms a weak hydrogen bond with the oxazole hydrogen. Nonetheless, substituting **15** for **16** leads to an energy gain of 13.4 kJ/mol in the binding energy (Table 4). This example validates potentially replacing weak hydrogen bonds with sulfur−oxygen interactions.

CONCLUSIONS

This paper has presented model system calculations and statistical analysis of S···O interactions in the PDB demonstrating that intermolecular S···O interactions between sulfur-containing aromatic rings and carbonyl oxygens, which have been largely overlooked in molecular modeling and drug design, are indeed favorable interactions. The M06-2X-D3/6-31++G** calculations showed that S···O contacts between thiophene or thiazole and a carbonyl oxygen (−21.8 to −23.0 kJ/mol) are comparable in strength to a typical hydrogen bond (i.e., water dimer) and that the strongest S···O contact observed in the thiadiazole model system (−26.9 kJ/mol) is similar in strength to a typical hydrogen bond (i.e., NH_3···OH_2). In addition, the nature of the intermolecular S···O interactions in the theoretical models was investigated. Potential energy scans revealed that all three S···O model systems can form complexes with very similar optimal S···O distances, σ-bond angles, and spherical angles, and practical guides for computational biologists and medicinal chemists were derived. A comprehensive analysis of structural information extracted from the PDB indicates that sp^2-hybridized sulfur can interact with oxygens in carbonyl, hydroxyl, and carboxylic acid groups. The geometry data from the PDB were projected onto a geometry−energy map, and many of the S···O contacts fall in the medium- and high-strength regions of the map. Several typical examples based on the projection have been discussed. Intriguingly, favorable intermolecular S···O interactions are observed in various drug targets. The theoretical results can be used to identify favorable regions for S···O interactions in binding sites and to perform scaffold hopping or de novo design. Three cases in which ligand moieties were replaced by thiazole or thiophene and the resulting bioactivities were published were found in the literature, and QM/MM calculations of the structures were performed. The results indicated that intermolecular S···O interactions not only improve the compound binding affinity but also might help to tune its selectivity. This work provides insight into sulfur-containing scaffolds and new approaches for lead optimization in medicinal chemistry. In this work, the intermolecular S···O interactions, which are still not included in scoring functions despite some recent force field modifications,[65] were not parametrized. This paper highlights the importance of this particular interaction and should motivate researchers to utilize it in regular drug discovery strategies. S···O, S···N, and S···S interactions are already receiving increasing attention from scientists.[66−69] Further interdisciplinary investigations will be required to fully understand and validate the potential of these interactions in biological systems.

ASSOCIATED CONTENT

Supporting Information

The Supporting Information is available free of charge on the ACS Publications website at DOI: 10.1021/acs.jcim.5b00177.

NCI analysis of the thiazole and *N*-methylacetamide model system (Figure S1), comparison of complex formation energies and interaction geometries obtained using different QM methods (Table S1), dipole moments of the three different sulfur-containing aromatic rings (Table S2), and a summary of the results of the distance scans (Table S3) (PDF)

AUTHOR INFORMATION

Corresponding Authors

*E-mail: jian_li@wuxiapptec.com Phone: +86-021-50464625.
*E-mail: lutao@cpu.edu.cn Phone: +86-025-86185086.

Funding

This work was supported by grants from National Basic Research Program of China (973 program, 2012CB724500).

Notes

The authors declare no competing financial interest.

ACKNOWLEDGMENTS

We are grateful for the precious suggestions given by associates, especially Dr. Fei Wang, from Computer-Aided Drug Design Lab of WuXi AppTec.

REFERENCES

(1) DasGupta, N. K.; Birss, F. W. π-Electron Structure of Heterocyclic Molecules Containing Sulfur. *Tetrahedron* **1980**, *36*, 2711−2720.
(2) Huber, R. G.; Margreiter, M. A.; Fuchs, J. E.; von Grafenstein, S.; Tautermann, C. S.; Liedl, K. R.; Fox, T. Heteroaromatic Π-Stacking Energy Landscapes. *J. Chem. Inf. Model.* **2014**, *54*, 1371−1379.
(3) Bissantz, C.; Kuhn, B.; Stahl, M. A Medicinal Chemist's Guide to Molecular Interactions. *J. Med. Chem.* **2010**, *53*, 5061−5084.
(4) Kucsman, Á.; Kapovits, I.; Párkányi, L.; Argay, G.; Kálmán, A. Intramolecular sulphur(II)—oxygen Interaction in Sulphides and Disulphides with 2-Methoxycarbonylphenyl and 2-Nitrophenyl Groups: An X-Ray Study. *J. Mol. Struct.* **1984**, *125*, 331−347.
(5) Burling, F. T.; Goldstein, B. M. Computational Studies of Nonbonded Sulfur-Oxygen and Selenium-Oxygen Interactions in the Thiazole and Selenazole Nucleosides. *J. Am. Chem. Soc.* **1992**, *114*, 2313−2320.
(6) Ángyán, J. G.; Kucsman, Á.; Poirier, R. A.; Csizmadia, I. G. Intramolecular Sulfur—oxygen Interaction: An Ab Initio Conformational Study of (Z)-3-Fluorothio-2-Propenal. *J. Mol. Struct.: THEOCHEM* **1985**, *123*, 189−201.
(7) Murray, J. S.; Lane, P.; Politzer, P. Simultaneous Sigma-Hole and Hydrogen Bonding by Sulfur- and Selenium-Containing Heterocycles. *Int. J. Quantum Chem.* **2008**, *108*, 2770−2781.
(8) Rosenfield, R. E.; Parthasarathy, R.; Dunitz, J. D. Directional Preferences of Nonbonded Atomic Contacts with Divalent Sulfur. 1. Electrophiles and Nucleophiles. *J. Am. Chem. Soc.* **1977**, *99*, 4860−4862.
(9) Kucsman, A.; Kapovits, I. Nonbonded Sulfur-Oxygen Interaction in Organic Sulfur Compounds. *Stud. Org. Chem.* **1985**, *19*, 191−245.
(10) Markham, G. D.; Bock, C. W. Intramolecular Sulfur-Oxygen Interactions: An Ab Initio Molecularorbital and Density Functional

DOI: 10.1021/acs.jcim.5b00177
J. Chem. Inf. Model. 2015, 55, 2138−2153

Theory Investigation. *J. Mol. Struct.: THEOCHEM* **1997**, *418*, 139−154.
(11) Iwaoka, M.; Takemoto, S.; Tomoda, S. Statistical and Theoretical Investigations on the Directionality of Nonbonded S···O Interactions. Implications for Molecular Design and Protein Engineering. *J. Am. Chem. Soc.* **2002**, *124*, 10613−10620.
(12) Beno, B. R.; Yeung, K.-S.; Bartberger, M. D.; Pennington, L. D.; Meanwell, N. A. A Survey of the Role of Noncovalent Sulfur Interactions in Drug Design. *J. Med. Chem.* **2015**, *58*, 4383−4438.
(13) Iwaoka, M.; Takemoto, S.; Okada, M.; Tomoda, S. Statistical Characterization of Nonbonded S···O Interactions in Proteins. *Chem. Lett.* **2001**, *2*, 132−133.
(14) Taylor, R. D.; MacCoss, M.; Lawson, A. D. G. Rings in Drugs. *J. Med. Chem.* **2014**, *57*, 5845−5859.
(15) Cortellis. https://cortellis.thomsonreuterslifesciences.com/ngg/home.do/ (accessed March 1, 2015).
(16) Berman H. M.; Westbrook J.; Feng Z.; Gilliland G.; Bhat T. N.; Weissig H.; Shindyalov I. N.; Bourne P. E. The Protein Data Bank. http://www.rcsb.org/ (accessed Dec 31, 2014).
(17) Ilardi, E. A.; Vitaku, E.; Njardarson, J. T. Data-Mining for Sulfur and Fluorine: An Evaluation of Pharmaceuticals To Reveal Opportunities for Drug Design and Discovery. *J. Med. Chem.* **2014**, *57*, 2832−2842.
(18) Li, Y.; Geng, J.; Liu, Y.; Yu, S.; Zhao, G. Thiadiazole-A Promising Structure in Medicinal Chemistry. *ChemMedChem* **2013**, *8*, 27−41.
(19) *Jaguar*, version 8.5; Schrödinger, LLC: New York, 2014.
(20) Glendening, E. D.; Badenhoop, J. K.; Reed, A. E.; Carpenter, J. E.; Bohmann, J. A.; Morales, C. M.; Landis, C. R.; Weinhold, F.; *NBO*, version 6.0; Theoretical Chemistry Institute, University of Wisconsin: Madison, WI, 2013.
(21) Zhao, Y.; Truhlar, D. G. The M06 Suite of Density Functionals for Main Group Thermochemistry, Thermochemical Kinetics, Noncovalent Interactions, Excited States, and Transition Elements: Two New Functionals and Systematic Testing of Four M06-Class Functionals and 12 Other Function. *Theor. Chem. Acc.* **2008**, *120*, 215−241.
(22) Grimme, S. Improved Second-Order Møller-Plesset Perturbation Theory by Separate Scaling of Parallel- and Antiparallel-Spin Pair Correlation Energies. *J. Chem. Phys.* **2003**, *118*, 9095−9102.
(23) Grimme, S.; Antony, J.; Ehrlich, S.; Krieg, H. A Consistent and Accurate Ab Initio Parametrization of Density Functional Dispersion Correction (DFT-D) for the 94 Elements H-Pu. *J. Chem. Phys.* **2010**, *132*, 154104.
(24) Hariharan, P. C.; Pople, J. A. The Influence of Polarization Functions on Molecular Orbital Hydrogenation Energies. *Theor. Chim. Acta.* **1973**, *28*, 213−222.
(25) Francl, M. M.; Pietro, W. J.; Hehre, W. J.; Binkley, J. S.; Gordon, M. S.; DeFrees, D. J.; Pople, J. A. Self-Consistent Molecular Orbital Methods. XXIII. A Polarization-Type Basis Set for Second-Row Elements. *J. Chem. Phys.* **1982**, *77*, 3654−3665.
(26) Hehre, W. J.; Ditchfield, R.; Pople, J. A. Self-Consistent Molecular Orbital Methods. XII. Further Extensions of Gaussian—Type Basis Sets for Use in Molecular Orbital Studies of Organic Molecules. *J. Chem. Phys.* **1972**, *56*, 2257−2261.
(27) Binkley, J. S.; Pople, J. A. Self-consistent Molecular Orbital Methods. XIX. Splitvalence Gaussiantype Basis Sets for Beryllium. *J. Chem. Phys.* **1977**, *66*, 879−880.
(28) Ditchfield, R.; Hehre, W. J.; Pople, J. A. Self-Consistent Molecular-Orbital Methods. IX. An Extended Gaussian-Type Basis for Molecular-Orbital Studies of Organic Molecules. *J. Chem. Phys.* **1971**, *54*, 724.
(29) Hehre, W. J.; Pople, J. A. Self-Consistent Molecular Orbital Methods. XIII. An Extended Gaussian-Type Basis for Boron. *J. Chem. Phys.* **1972**, *56*, 4233−4234.
(30) Boys, S. F.; Bernardi, F. The Calculation of Small Molecular Interactions by the Differences of Separate Total Energies. Some Procedures with Reduced Errors. *Mol. Phys.* **1970**, *19*, 553−566.
(31) Clark, T.; Chandrasekhar, J.; Spitznagel, G. W.; Schleyer, P. V. R. Efficient Diffuse Function-Augmented Basis Sets for Anion Calculations. III. The 3-21+G Basis Set for First-Row Elements, Li−F. *J. Comput. Chem.* **1983**, *4*, 294−301.
(32) Krishnan, R.; Binkley, J. S.; Seeger, R.; Pople, J. A. Self-Consistent Molecular Orbital Methods. XX. A Basis Set for Correlated Wave Functions. *J. Chem. Phys.* **1980**, *72*, 650.
(33) Frisch, M. J.; Pople, J. A.; Binkley, J. S. Self-Consistent Molecular Orbital Methods 25. Supplementary Functions for Gaussian Basis Sets. *J. Chem. Phys.* **1984**, *80*, 3265.
(34) McLean, A. D.; Chandler, G. S. Contracted Gaussian Basis Sets for Molecular Calculations. I. Second Row Atoms, Z = 11−18. *J. Chem. Phys.* **1980**, *72*, 5639.
(35) Su, P.; Li, H. Energy Decomposition Analysis of Covalent Bonds and Intermolecular Interactions. *J. Chem. Phys.* **2009**, *131*, 014102.
(36) Chen, W.; Gordon, M. S. Energy Decomposition Analyses for Many-Body Interaction and Applications to Water Complexes. *J. Phys. Chem.* **1996**, *100*, 14316−14328.
(37) Schmidt, M. W.; Baldridge, K. K.; Boatz, J. A.; Elbert, S. T.; Gordon, M. S.; Jensen, J. J.; Koseki, S.; Matsunaga, N.; Nguyen, K. A.; Su, S.; Windus, T. L.; Dupuis, M.; Montgomery, J. A. General atomic and molecular electronic structure system. *J. Comput. Chem.* **1993**, *14*, 1347−1363.
(38) *QSite*, version 6.2; Schrödinger, LLC: New York, 2014.
(39) *Prime*, version 3.6; Schrödinger, LLC: New York, 2014.
(40) Hornak, V.; Abel, R.; Okur, A.; Strockbine, B.; Roitberg, A.; Simmerling, C. Comparison of Multiple Amber Force Fields and Development of Improved Protein Backbone Parameters. *Proteins: Struct., Funct., Genet.* **2006**, *65*, 712−725.
(41) Kaminski, G. A.; Friesner, R. A.; Tirado-Rives, J.; Jorgensen, W. L. Evaluation and Reparametrization of the OPLS-AA Force Field for Proteins via Comparison with Accurate Quantum Chemical Calculations on Peptides. *J. Phys. Chem. B* **2001**, *105*, 6474−6487.
(42) Hay, P. J.; Wadt, W. R. Ab Initio Effective Core Potentials for Molecular Calculations. Potentials for the Transition Metal Atoms Sc to Hg. *J. Chem. Phys.* **1985**, *82*, 270−283.
(43) Wadt, W. R.; Hay, P. J. Ab Initio Effective Core Potentials for Molecular Calculations. Potentials for Main Group Elements Na to Bi. *J. Chem. Phys.* **1985**, *82*, 284−298.
(44) *PyMOL*, version 1.5.0.4; Schrödinger, LLC: New York, 2014.
(45) PyMOL Wiki. http://www.pymolwiki.org/ (accessed Dec 31, 2014).
(46) *Maestro*, version 9.4; Schrödinger, LLC: New York, 2014.
(47) Wang, J.-F.; Feng, J.-K. Theoretical Studies of the Structures and Optical Properties of the Bifluorene and Its Derivatives. *J. Phys. Org. Chem.* **2007**, *20*, 130−137.
(48) Chen, Y.; Shoichet, B.; Bonnet, R. Structure, Function, and Inhibition along the Reaction Coordinate of CTX- B-Lactamases. *J. Am. Chem. Soc.* **2005**, *127*, 5423−5434.
(49) Davies, D. R.; Mamat, B.; Magnusson, O. T.; Christensen, J.; Haraldsson, M. H.; Mishra, R.; Pease, B.; Hansen, E.; Singh, J.; Zembower, D.; Kim, H.; Kiselyov, A. S.; Burgin, A. B.; Gurney, M. E.; Stewart, L. J. Discovery of Leukotriene A4 Hydrolase Inhibitors Using Metabolomics Biased Fragment Crystallography. *J. Med. Chem.* **2009**, *52*, 4694−4715.
(50) Bénardeau, A.; Benz, J.; Binggeli, A.; Blum, D.; Boehringer, M.; Grether, U.; Hilpert, H.; Kuhn, B.; Märki, H. P.; Meyer, M.; Püntener, K.; Raab, S.; Ruf, A.; Schlatter, D.; Mohr, P. Aleglitazar, a New, Potent, and Balanced Dual PPARα/γ Agonist for the Treatment of Type II Diabetes. *Bioorg. Med. Chem. Lett.* **2009**, *19*, 2468−2473.
(51) Huang, X.; Cheng, C. C.; Fischmann, T. O.; Duca, J. S.; Yang, X.; Richards, M.; Shipps, G. W. Discovery of a Novel Series of Chk1 Kinase Inhibitors with a Distinctive Hinge Binding Mode. *ACS Med. Chem. Lett.* **2012**, *3*, 123−128.
(52) Wang, Y.; Kirschner, A.; Fabian, A. K.; Gopalakrishnan, R.; Kress, C.; Hoogeland, B.; Koch, U.; Kozany, C.; Bracher, A.; Hausch, F. Increasing the Efficiency of Ligands for FK506-Binding Protein 51 by Conformational Control. *J. Med. Chem.* **2013**, *56*, 3922−3935.

DOI: 10.1021/acs.jcim.5b00177
J. Chem. Inf. Model. 2015, 55, 2138−2153

(53) Ellis, D. A.; Blazel, J. K.; Webber, S. E.; Tran, C. V.; Dragovich, P. S.; Sun, Z.; Ruebsam, F.; McGuire, H. M.; Xiang, A. X.; Zhao, J.; Li, L. S.; Zhou, Y.; Han, Q.; Kissinger, C. R.; Showalter, R. E.; Lardy, M.; Shah, A. M.; Tsan, M.; Patel, R.; LeBrun, L. A.; Kamran, R.; Bartkowski, D. M.; Nolan, T. G.; Norris, D. A.; Sergeeva, M. V.; Kirkovsky, L. 4-(1,1-Dioxo-1,4-Dihydro-1λ^6-Benzo[1,4]Thiazin-3-Yl)-5-Hydroxy-2H-Pyridazin-3-Ones as Potent Inhibitors of HCV NS5B Polymerase. *Bioorg. Med. Chem. Lett.* **2008**, *18*, 4628−4632.
(54) Sun, F.; Huo, X.; Zhai, Y.; Wang, A.; Xu, J.; Su, D.; Bartlam, M.; Rao, Z. Crystal Structure of Mitochondrial Respiratory Membrane Protein Complex II. *Cell* **2005**, *121*, 1043−1057.
(55) Dawson, A.; Tulloch, L. B.; Barrack, K. L.; Hunter, W. N. High-Resolution Structures of Trypanosoma Brucei Pteridine Reductase Ligand Complexes Inform on the Placement of New Molecular Entities in the Active Site of a Potential Drug Target. *Acta Crystallogr., Sect. D: Biol. Crystallogr.* **2010**, *66*, 1334−1340.
(56) Sevrioukova, I. F.; Poulos, T. L. Dissecting Cytochrome P450 3A4-Ligand Interactions Using Ritonavir Analogues. *Biochemistry* **2013**, *52*, 4474−4481.
(57) DeLaBarre, B.; Gross, S.; Fang, C.; Gao, Y.; Jha, A.; Jiang, F.; Song J., J.; Wei, W.; Hurov, J. B. Full-Length Human Glutaminase in Complex with an Allosteric Inhibitor. *Biochemistry* **2011**, *50*, 10764−10770.
(58) Chan, C.; Borthwick, A. D.; Brown, D.; Burns-Kurtis, C. L.; Campbell, M.; Chaudry, L.; Chung, C.; Convery, M. A.; Hamblin, J. N.; Johnstone, L.; Kelly, H. A.; Kleanthous, S.; Patikis, A.; Patel, C.; Pateman, A. J.; Senger, S.; Shah, G. P.; Toomey, J. R.; Watson, N. S.; Weston, H. E.; Whitworth, C.; Young, R. J.; Zhou, P. Factor Xa Inhibitors: S1 Binding Interactions of a Series of N-{(3S)-1-[(1S)-1-Methyl-2-Morpholin-4-Yl-2-Oxoethyl]-2-Oxopyrrolidin-3-Yl}-sulfonamides. *J. Med. Chem.* **2007**, *50*, 1546−1557.
(59) Blagg, J. A.; Noe, M. C.; Wolf-Gouveia, L. A.; Reiter, L. A.; Laird, E. R.; Chang, S. P. P.; Danley, D. E.; Downs, J. T.; Elliott, N. C.; Eskra, J. D.; Griffiths, R. J.; Hardink, J. R.; Haugeto, A. I.; Jones, C. S.; Liras, J. L.; Lopresti-Morrow, L. L.; Mitchell, P. G.; Pandit, J.; Robinson, R. P.; Subramanyam, C.; Vaughn-Bowser, M. L.; Yocum, S. A. Potent Pyrimidinetrione-Based Inhibitors of MMP-13 with Enhanced Selectivity over MMP-14. *Bioorg. Med. Chem. Lett.* **2005**, *15*, 1807−1810.
(60) Geng, B.; Basarab, G.; Comita-Prevoir, J.; Gowravaram, M.; Hill, P.; Kiely, A.; Loch, J.; MacPherson, L.; Morningstar, M.; Mullen, G.; Osimboni, E.; Satz, A.; Eyermann, C.; Lundqvist, T. Potent and Selective Inhibitors of Helicobacter Pylori Glutamate Racemase (MurI): Pyridodiazepine Amines. *Bioorg. Med. Chem. Lett.* **2009**, *19*, 930−936.
(61) Gogonea, V.; Suárez, D.; van der Vaart, A.; Merz, K. M., Jr. New Developments in Applying Quantum Mechanics to Proteins. *Curr. Opin. Struct. Biol.* **2001**, *11*, 217−223.
(62) Murphy, R. B.; Philipp, D. M.; Friesner, R. A. A Mixed Quantum Mechanics/molecular Mechanics (QM/MM) Method for Large-Scale Modeling of Chemistry in Protein Environments. *J. Comput. Chem.* **2000**, *21*, 1442−1457.
(63) Philipp, D. M.; Friesner, R. A. Mixed Ab Initio QMrMM Modeling Using Dipeptide and Tetrapeptide. *J. Comput. Chem.* **1999**, *20*, 1468−1494.
(64) Murphy, R. B.; Philipp, D. M.; Friesner, R. A. Frozen Orbital QM/MM Methods for Density Functional Theory. *Chem. Phys. Lett.* **2000**, *321*, 113−120.
(65) Lupyan, D.; Abramov, Y. A.; Sherman, W. Close Intramolecular Sulfur-Oxygen Contacts: Modified Force Field Parameters for Improved Conformation Generation. *J. Comput.-Aided Mol. Des.* **2012**, *26*, 1195−1205.
(66) Jalsovszky, I.; Farkas, Ö.; Kucsman, Á. Transannular Sulfur-Nitrogen Interactions in Stereoisomeric 1,5-Thiazocine Derivatives: An Ab Initio MO Study. *J. Mol. Struct.: THEOCHEM* **1997**, *418*, 155−163.
(67) Iwaoka, M.; Isozumi, N. Possible Roles of S···O and S···N Interactions in the Functions and Evolution of Phospholipase A2. *Biophysics (Biophys. Soc. Jpn.)* **2006**, *2*, 23−34.
(68) Adhikari, U.; Scheiner, S. Effects of Charge and Substituent on the S···N Chalcogen Bond. *J. Phys. Chem. A* **2014**, *118*, 3183−3192.
(69) Nagy, P.; Szabó, D.; Kapovits, I.; Kucsman, Á.; Argay, G.; Kálmán, A. Intramolecular S···S and S···O Close Contacts in 1,8-Bis(phenylsulfanyl)naphthalene Derivatives of Different Sulfur Valence State: An X-Ray Study. *J. Mol. Struct.* **2002**, *606*, 61−76.

DOI: 10.1021/acs.jcim.5b00177
J. Chem. Inf. Model. 2015, 55, 2138−2153